SKB
ÄSPÖLABORATORIET

INTERNATIONAL COOPERATION REPORT 94-14

Hydrodynamic modelling of the Äspö HRL

Discrete fracture model

D Billaux
ITASCA

F Guérin, J Wendling
ANTEA

November 1994

Supported by ANDRA, France

SVENSK KÄRNBRÄNSLEHANTERING AB
SWEDISH NUCLEAR FUEL AND WASTE MANAGEMENT CO

BOX 5864 S-102 40 STOCKHOLM

TEL. +46-8-665 28 00 TELEX 13108 SKB TELEFAX +46-8-661 57 19

ISSN 1104-3210
ISRN SKB-ICR--94/14--SE

HYDRODYNAMIC MODELLING OF THE ÄSPÖ HRL

DISCRETE FRACTURE MODEL

D Billaux
ITASCA

F Guérin, J Wendling
ANTEA

November 1994

Supported by ANDRA, France

HYDRODYNAMIC MODELLING OF THE ÄSPÖ HRL

DISCRETE FRACTURE MODEL

D Billaux
ITASCA

F Guérin, J Wendling
ANTEA

November 1994

Supported by ANDRA, France

TABLE OF CONTENTS

EXECUTIVE SUMMARY

The Äspö Hard Rock Laboratory (HRL) is being constructed in preparation for the deep geological repository of high-level nuclear waste in Sweden. ANDRA signed a cooperation agreement with SKB, the Swedish Nuclear Fuel and Waste Management Company. This includes participation in a Task Force on Modelling of Groundwater Flow and Transport of Solutes. As part of its involvement in this Task Force, ANDRA has asked several french teams to model a 92 days-long pumping and tracer test named LPT2. This report presents the modelling effort by an ITASCA Consultants-BRGM team.

The model assumes that all flow and transport take place in a network of one-dimensional channels. A geometrical study is first performed. The extension of fractures zones is assessed from available data on borehole intersections. The connectivity of the average rock outside fracture zones is studied using fracture traces mapped in part of the access drift. This study shows that the average rock is connected : flow paths may exist at site scale outside fracture zones. However, representing these flow paths by an equivalent porous medium is likely to be erroneous.

A parameter study of the influence of fracture zone transmissivity contrasts on the drawdown field at the end of the pumping test shows that the results of the test provide enough information to constrain, within one order of magnitude, the transmissivityof eight out of the ten zones most influenced by the pumping. However a few zones situated close to the test cannot be characterized properly. In order to gain a non- ambiguous knowledge of the large scale conductors properties in a site such as Äspö, two or three pumping tests such as LPT2 would probably be necessary.

Transient-state simulations of the test were performed, first assuming flow is restricted in fracture zones, then taking into account the storage effect of the average rock. Fracture zones-only storage can explain the response of the system during the first ten days. However, average rock storage must be taken into account to reproduce the evolution of drawdowns at later times. This was done by adding to the fracture zones channel network a sparse three-dimensionnal regular grid. Such an approach produces drawdown curves close to the measured ones, except for a few notable exceptions, and properly accounts for the discrete nature of flow.

Preliminary tracer transport simulations were aimed at assessing the suitability of the channel model for modelling a large scale tracer test. A breakthrough curve was correctly reproduced. However the model cannot simulate tracer losses.

The channel network model we used, because it is very flexible, allowed a number of parametric studies. This is the main advantage of such a model, and makes it particularly useful during the first phases of a site investigation, when many still valid hypotheses must be tested.

1 INTRODUCTION

A large research programme is carried out in Sweden before the construction of a final repository for high level nuclear waste. In this framework, an underground laboratory project, in the Äspö island (South-Eastern Sweden) was started in 1986.

Geophysical and borehole investigations were performed. Among them, a 90-days long pumping test, named LPT2, was carried out at the end of 1990.

Modelling this test was assigned as Task 1 by the international Task Force on groundwater flow and transport of solutes. This report presents a channeled discrete-fracture model of the site. The geometry of the fracture zones network is first determined. We then study the "average rock" fracture connectivity. LPT2 is then simulated. Using drawdowns at the end of the pumping phase, and considering them as a steady state, we first investigate the effect of fracture zone transmissivity contrasts on the drawdown field. For the transient simulations that follow, two hypotheses are considered : either water storage occurs only in the fracture zones, or storage is distributed between fracture zones and the average rock. Finally, preliminary transport simulations are performed.

2 GEOMETRICAL STUDY

2.1 FRACTURE ZONES NETWORK

The fracture field in Äspö is characterized by its strong heterogeneity. Fractures are clustered in large fracture zones, with a size varying from hundreds to thousands of meters. Their traces at ground surface are at least partly mapped by surface investigations, while their position underground can be inferred by intersections with boreholes.

We represent each fracture zone by one plane. The intersections of this plane with the ground surface and boreholes are in agreement with observations. This plane is supposed to be a disk. However, channeled flow in the fracture zone may be restricted further by model boundaries or any polygonal shape.

Fracture planes positions and orientations were given by the HRL team. We used the second geometry given to us (mail by Anders Ström, Feb. 15, 1993, ref. 25.1078). Partial ground surface traces had to be completed, taking into account intersections with boreholes to assess the extension of a given zone. The EW1, EW3, and EW5 zones are the only ones left crossing the whole model (Figure 2-1). Figure 2-2 shows the fracture zone geometry in a 2400 m x 2400 m x 1240 m box. A regular channel grid is shown on each zone.

2.2 CONNECTIVITY OF THE "AVERAGE ROCK"

In order to assess the connectivity of the average rock, we use the results of fracture mapping in the first 750 m of the laboratory access drift. This section starts close to ground surface at a distance of about 1500 m from the laboratory and ends at a depth of 100 m and at a distance of 750 m from the laboratory. It is excavated essentially in the "Småland Granite", whereas the laboratory is in the "Äspö Diorite".

Fracture mapping data were pre-processed by Munier /Munier, 1993/, and we use his paper as a starting point. Two fracture sets are defined, one being sub-vertical and one sub-horizontal. From observed trace lengths, assuming a log-normal disk radius distribution, the parameters of this distribution can be calculated. They are then verified by generating disk networks with the obtained radius

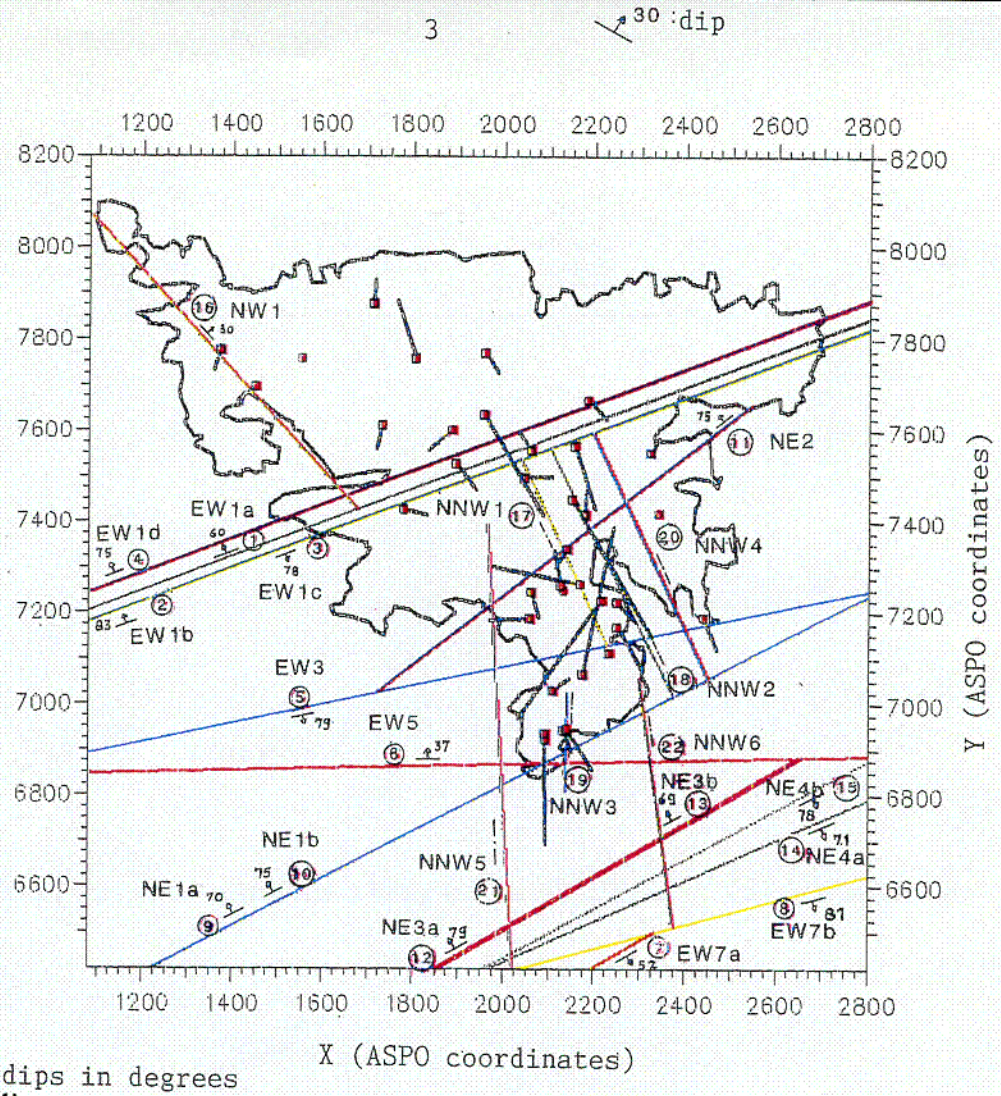

- dips in degrees
- Äspo coordinates in metres

Figure 2-1. Completed surface traces of fracture zones.

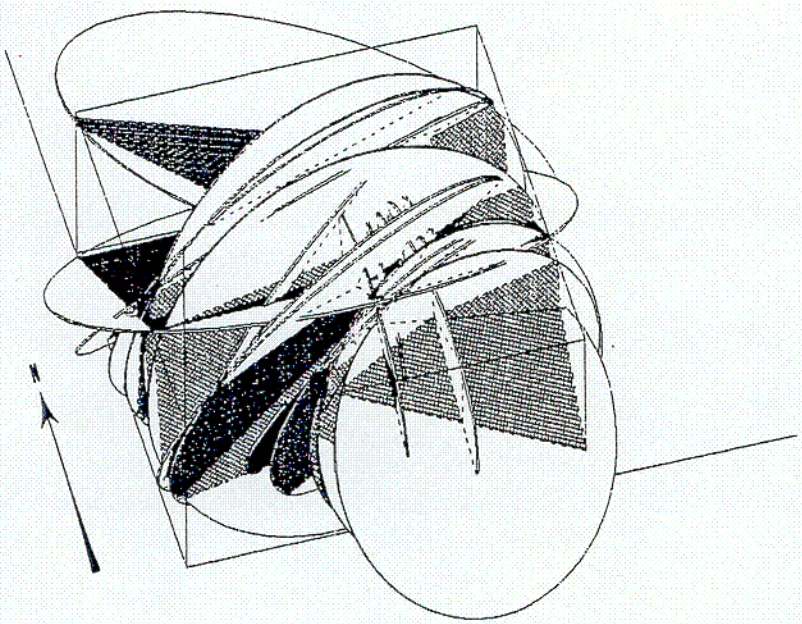

Figure 2-2. Network used for optimizations.

C-01

Only fractures noted as "water bearing" are used for these computations. The resulting radius distribution has a mean of 1.85 m and a standard deviation of 0.6 m.

The density of the fracture network is computed from the number of water-bearing fractures on a sampling line parallel to the access drift axis. The volumic density of a fracture field required to produce a given number of intersections with a sampling line can readily be computed, given the orientation of the line, the orientation and the size distributions of the fractures :

$$\lambda_V \cdot \cos\theta \cdot S = \lambda_1$$

where :

λ_V is the volumic density (m^{-3});
$\cos\theta$ is the average cosine of angle θ between the sampling line and fracture poles ;
S is the mean fracture area ;
λ_1 is the density of intersections on the sampling line (m^{-1}).

However, applying this to water-bearing fractures largely underestimates the true density : a fracture field generated this way will have a low connectivity and therefore will contain many isolated fractures. These isolated fractures cannot be water bearing, so we create a network with a density of water bearing fractures far smaller than the computed density. In fact, using the above expression, we obtain densities of 1.2 $10^{-2}m^{-3}$ for both horizontal and vertical fracture sets. A network with such densities generated in a 180 m-diameter sphere contains about 80 % of isolated fractures. We therefore resort to trial and error to find the fracture set densities reproducing the sampling line observations. Densities of 1.8 $10^{-2}m^{-3}$ are found adequate.

Using the network statistics, we compute a Connectivity Index defined as the mean number of intersections per fracture, weighted by fracture diameter. This is a good indicator of network connectivity /Guérin and Billaux, 1993/. A network is likely to percolate, i.e. to support flow at any scale, if its Connectivity Index is above a given critical value. This value is 2 if fracture orientations are totally random, and becomes 3.2 if all fractures have a direction in common /Robinson, 1984/.

For the Äspö average rock, we find an Index of 2.6. Fractures are therefore poorly connected, but still allow some large scale flow. However, assimilating the fracture field with an equivalent porous medium seems hazardous. The Representative Elementary Volume for such a network is much larger than the 180 m-diameter sphere we studied.

The simulations shown in chapter 3 assume that "average rock" flow can be neglected and therefore deal only with fractures zones. For transient simulations, in chapter 4, we then present a crude representation of the average rock storage effect.

3 DRAWDOWNS AT THE END OF LPT2-STEADY STATE SIMULATIONS

In this chapter, we study the hydraulic state of the site at the end of the 92 days pumping test, assuming that a steady state has been achieved. Our aim here is to assess how well a transmissivity field can be deduced from the model assumptions and the experimental data. For the couple (model - experiment) to yield a robust characterisation of the site, we need both a valid model and an experiment which effectively affected most of the system.

We use a simple inverse modelling technique to optimize equivalent fracture zone transmissivities, and compare the results obtained with six sets of data weighting factors.

3.1 INVERSE MODELLING TECHNIQUE

Suppose a model with n parameters T_i, i = 1, n, that we wish to optimize. We have m measurements. We call $S = \Sigma\ S_j$, where the S_j are the square differences between the measurements and corresponding values simulated by the model, for a given set of T_i (the S_i values may eventually be assigned weighting factors).

We start with a first guess at the T_i. First, we fix all the T_k for $k \neq i$. We perform three computations, for three values of T_i separated by an interval δt_i. For these three values t_i, $t_i - \delta t_i$, $t_i + \delta t_i$, we can compute quadratic errors S_i, S_i^- and S_i^+. We can then evaluate the first and second order partial derivatives of S at point t_i :

$$\frac{\partial S}{\partial T_i} \approx \frac{s_i^+ - s_i^-}{2\delta t_i}$$

and

$$\frac{\partial^2 S}{\partial T_i^2} \approx \frac{s_i^+ + s_i^- - 2s_i}{\delta t_i^{\,2}}$$

If the second order derivative at t_i is positive, we assume this derivative is a constant around t_i, and compute the point t_{io} where the first deritative is zero :

$$t_{io} = t_i - \left(\frac{\partial S}{\partial T_i} / \frac{\partial^2 S}{\partial T_i^2}\right)$$

In order to avoid too large extrapolations, we limit the absolute difference between t_i and t_{io} at twice the value of the interval δt_i.

Once t_{io} is choosen, we perform a new computation to evaluate the corresponding quadratic error S. If S increases when T_i goes from t_i to t_{io}, the t_{io} value is rejected and the interval δt_i is divided by two, since in this case we know there is a minimum of S between t_i and t_{io}. This interval is also halved if the difference between t_i and t_{io} is less than $\delta t_i/10$.

If the second order deritative is negative, we set t_{io} to the value, among (t_i, $t_i - \delta t_i$, $t_i + \delta t_i$) which gives the smallest error S.

We then go to the next parameter T_{i+1}. Note that the value of S at point t_{i+1} is already known : it is the value we just computed at point t_i for parameter T_i. Thus we need three simulations per parameter. Once the n parameters have been reviewed, the procedure is repeated until the value of the quadratic error becomes lower than a given tolerance, or this value does not change any more from one iteration to the other.

To model the Äspö site, we use fracture zones with regular square grids of channels. We assume that channel conductances are uniform within a zone, but may vary from zone to zone. The Ti parameters we chose for optimization are the conductances Ci of the zone channels. Since we want to "explore" several orders of magnitude, and keep positive values, we chose to optimize the logarithms of the C_i's.

The optimization algorithm is implemented in the CHANNET (CHANel NETworks) set of programs. This chain of codes dedicated to discrete fracture flow modelling was initially developped in Lawrence Berkeley Laboratory (programs FMG3D, TRINET for example) and then extensively improved by BRGM and ITASCA, during the last five years.

3.2 SPECIFICATIONS FOR THE MODELLING OF LPT2

3.2.1 Geometry and boundary conditions

The geometry of the fracture zones we use is the one described in paragraph 2.1.

The square channel grid on each zone has a 25 m edge L. Such a network produces an isotropic equivalent transmissivity τ :

$$\tau = C/L$$

where C is the conductance of the channels.

The boundary conditions are a zero imposed head on the four vertical faces, a zero imposed flux on the lower horizontal face, and a mixed condition on the upper horizontal face :

- within the Äspö island, an imposed flux reproduces the effect of water recharge. We use a total flowrate of 13.5 m3/day, which corresponds to steady-state calibrations (before pumping) by U. Svensson /Svensson, 1990/ and a BRGM team /Fillion and Noyer, 1994/. This flow rate is distributed uniformly among the zone traces inside the island.

- outside the island, a zero imposed head is used. In order to limit the influence of water inflow from the sea, since Äspö is very much enclosed by land, we use a kind of "skin effect" at the interface between the sea and the fracture zones : the conductance of any channel in contact with the sea is set to 1/20 of the regular channel conductance in that zone. Note that these reduced conductances are not affected by later optimizations. The results presented in paragraph 3.3 all correspond to this hypothesis. However, in paragraph 3.4, we compare these results to an optimization assuming uniform channel conductances in each zone, and no "skin effect".

A last boundary condition is the imposed flow rate in the pumping borehole KAS06, 2.25 m^3s^{-1}. Note that we do not specify the relative weights of the inflows from the several zones intersected by the borehole.

3.2.2 Observation points and optimized zones

Since we model only fracture zones, we use borehole observation sections which effectively intersect the zones. For each observation section, we select in the mesh the node closest to the center of the section. Such a method has the advantage of giving one grid node for any observation section. However, it forces the connexion between the borehole and the zone. because of zone heterogeneity, such a connexion may not exist in some cases.

We classify the selected nodes into three categories. 23 of the nodes are very close to the real observation section and are situated in the zone identified by the investigations. Among these, we distinguish the 7 nodes in zone EW5 : this zone, which is intersected by KAS06, is well sampled and extensively influenced by the test. It is thus likely to be well characterized by the test. The three categories are then :

- the 7 nodes in EW5 with coordinates close to observation sections, called "EW5 nodes" ;

- the 16 nodes, also "well defined", but not in EW5, called "first order nodes" ;

- the 38 nodes for which an incertainty subsists, either because of their position or because of the zone they lie on. We call these "second order nodes".

We perform six complete optimizations, varying the relative weights of the three categories of observaton nodes, from uniform weights to very contrasted ones (table 3-1).

Table 3-1. Weights of the three observation node categories for each of the six optimisations.

	1	2	3	4	5	6
EW5	1	1	1	2	10	10
First order	1	1	1	1	1	1
Second order	1	0.8	0.2	0.2	0.2	0.0

A few preliminary tests helped us assessing which zones had the biggest influence on the value of the quadratic error S. EW5 is logically the most influent, then EW1c, EW3 and NE2. Finally, a third group is EW1a, EW1b, NE1a, NE1b, NW1 and NNW1. The channel conductances in the other zones have little effect on S. Each of the six optimizations is therefore performed in three phases. First, only zone EW5 is considered. Then, the new EW5 conductances are used as input for an optimization including EW5, EW1c, EW3 and NE2. Finally, the results of this second phase are used as input for an optimization including these four zones plus the six zones in the third group. Table 3-2 gives the equivalent transmissivities used at the start for all zones.

Table 3-2 Initial equivalent zone transmissivities for optimisations, and fixed equivalent transmissivities for non-optimised zones.

Optimised zones	EW1a	EW1b	EW1c	EW3	EW5	NE1a	NE1b	NE2	NW1	NNW1
Transmissivity (10^{-5} m^2/s)	2	0,05	0,05	0,05	2	10	10	0,4	6,7	1,5

Non-optimised zones	EW1d	EW7a	EW7b	NE3a	NE3b	NE4a	NE4b	NNW2	NNW3	NNW4
T (20^{-5} m^2/s)	0,05	7	7	1,5	1,5	16	16	1,5	2	4

Non-optimised zones	NNW5	NNW6
T (10^{-5} m^2/s)	5	5

After completing the optimizations, we check that the 12 remaining zones have a limited influence on the quadratic error : a fourth phase of optimization is added at the end of the "type 4" optimization. This phase, which includes all the zones, yields a 2 % only decrease of the error S, mainly due to zones NNW4 and NNW5.

3.3 RESULTS

Table 3-3 and figures 3-1 and 3-2 summarize the results. The first three columns of the table show the efficiency of each optimization. The total decrease of the quadratic error S varies from 58 % for optimization 1 to 85 % for optimization 6. In fact, most of this decrease occurs in the first phase of the optimizations which deals only with the EW5 zone. The last two phases then reduce S by 20 to 30 %. Column 4 in table 4-3 enables a comparison between the 6 optimizations. It shows for each of them the value of S computed with the weighting used for optimization 4 (EW5 : 2 ; first order : 1 ; second order : 0.2). The maximum difference here is less than 6 %. We can therefore consider that the 6 optimizations yield results of the same quality.

Table 3-3. Optimization results.

Optimization	Initial S m^2	S after EW5 optimization (m^2)	Final S m^2	S for optimization 4 (m^2)
1	15.19	8.09	6.42	3.01
2	14.72	7.56	5.96	2.94
3	11.91	4.34	3.18	2.86
4	11.42	3.94	2.83	2.83
5	10.15	2.50	2.03	2.94
6	9.41	1.65	1.36	3.01

Figure 3-1 shows the equivalent transmissivities obtained, for the 10 zones studied, by the six optimizations. Figure 3-2 groups, for the 48 observation nodes situated in the 10 zones studied, the errors (computed drawdown minus measured drawdown) for each optimization.

Only zone NE1a shows both minimal drawdown errors and a robust determination of transmissivity, the results of the six optimizations beeing almost identical. Six other zones (EW1a, EW1b, EW1c, EW5, NE1b and NW1) show fairly well constrained transmissivities, with variations smaller than an order of magnitude, and computed drawdowns close to the measured ones (+ or - 2m). The remaining three zones show not so satisfying results. One zero drawdown measured in EW3, 200m from the pumping test only, is not reproduced, inducing a 6m error. For this zone also, optimization 1 yields a transmissivity two orders of magnitude higher than the 5 other ones. Transmissivities for zone NE2 are very variable, however computed drawdowns are close to measured ones. As for NNW1, two large measured drawdowns (15m and 16m) are not reproduced and account for (-9 to -11m) errors. Note that the zero drawdown observation in EW3 is close to the intersection of this zone with NNW1 were the largest drawdowns are measured.

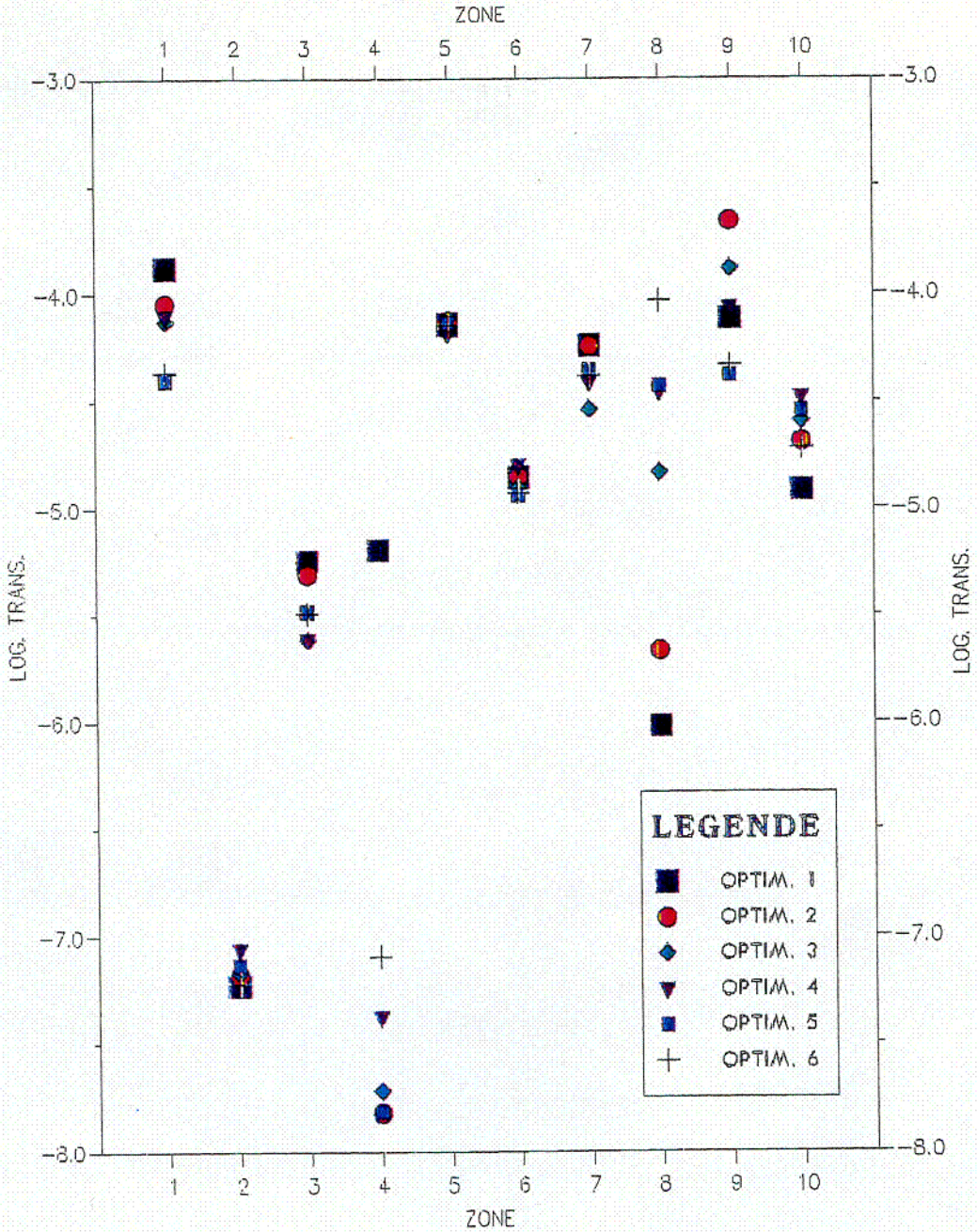

Optimized zones :

1/ EW1a	4/ EW3	7/ NE1b	10/NNW1
2/ EW1b	5/ EW5	8/ NE2	
3/ EW1c	6/ NE1a	9/ NW1	

Figure 3-1. Optimized transmissivities in zones.

C-02

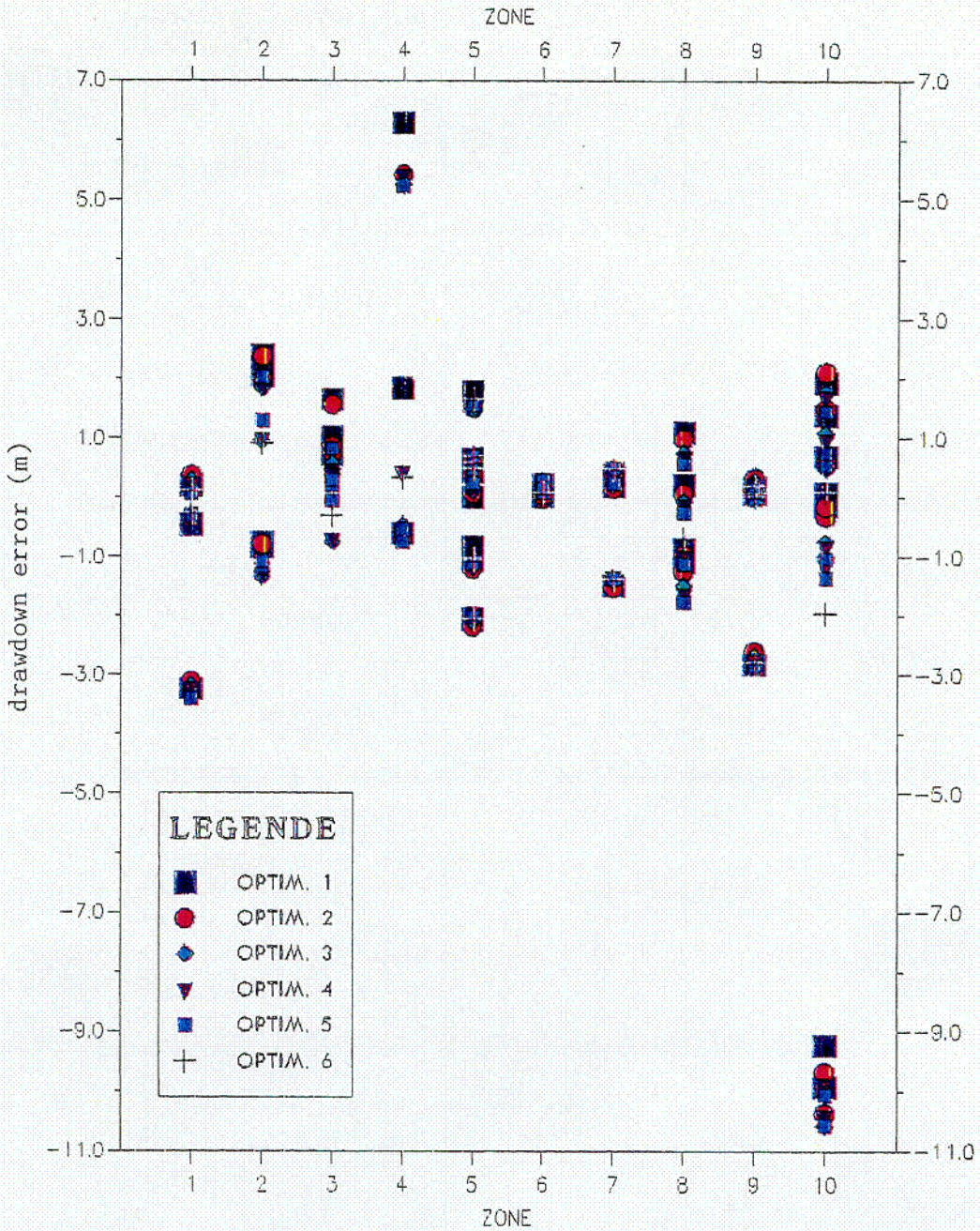

Optimized zones :

1/ EW1a	4/ EW3	7/ NE1b	10/NNW1
2/ EW1b	5/ EW5	8/ NE2	
3/ EW1c	6/ NE1a	9/ NW1	

Figure 3-2. Drawdown error in observation sections in optimized zones.

C-03

With the assumptions we use, i.e. uniform channel conductances within each zone, and systematic hydraulic connexion between any borehole and the zones it crosses, it is impossible to reproduce such contrasted responses.

Figure 3-3 shows the measured and computed drawdowns, for optimization 4, versus distance from the pumping well. Plots for the other five optimizations are very similar. The model tends to "smooth" drawdowns, the calculated values decreasing more regularly with distances than the measured ones.

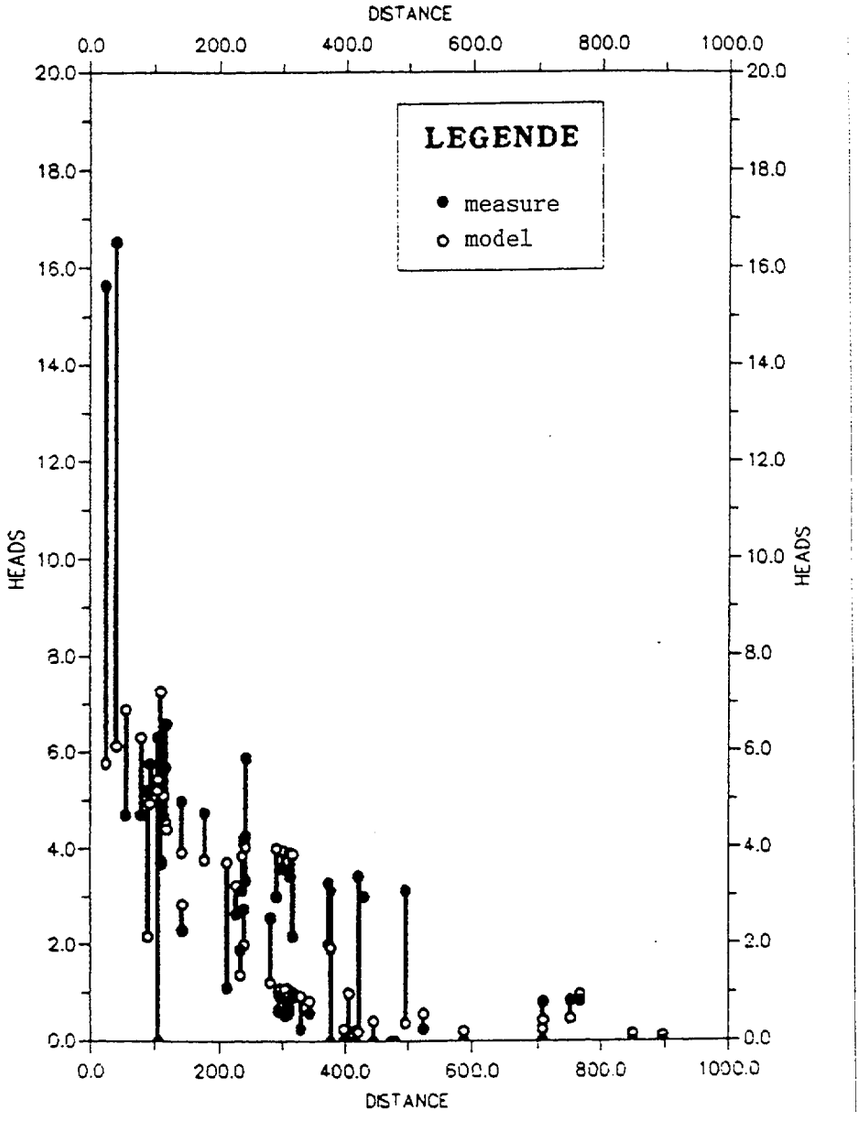

Figure 3-3. Observed and calculated drawdowns, optimization 4, versus distance from pumping well.

Table 3-4 shows the flowrates arriving in the pumping borehole KAS06. The model does not reproduce the inflow close to the ground surface from zone EW3. The transmissivity of EW3 does not seem to influence this result, since all inflows in EW3 are comparable, while its transmissivity varies from 6.5 10^{-6} m^2 s^{-1} (optimization 1) to 1.6 10^{-8} m^2 s^{-1} (optimization 5).

Table 3-4. Inflow rates, in percent.

Optimization	EW3	EW5	NNW2	NNW1
1	0.5	51.7	38.3	9.5
2	0.5	52.2	37.9	9.4
3	0.03	48.0	36.7	15.3
4	0.05	42.5	37.35	20.1
5	0.5	54.4	36.1	9.0
6	0.09	47.7	39.6	12.6
measured	16	34	28	22

The relative magnitudes of other inflows, from zones EW5, NNW2 and NNW1, are generally well reproduced, although the model tends to overestimate inflows from EW5 and underestimate inflows from NNW1. Optimization 4 is the one giving the best results. For later tracer transport modelling, we will use the transmissivities obtained by this optimization.

3.4 DISCUSSION

All the computations presented above neglect the effect of water density contrasts due to the salinity. The Äspö island underground is fed with fresh water at ground surface, with salted water (7g/l concentration) by the Baltic Sea, and contains waters with concentrations due to the much higher salinity of the Baltic Sea at earlier times. Over the domain we model, concentrations from 0 g/l to 21 g/l have been measured.

The CHANNET program chain has the capability of accounting for heterogeneities of the fluid density. However, this model is not fully coupled : we cannot compute the effect of hydrodynamics on the salinity field. In order to assess the magnitude of density effects, we use a salinity field computed by an other team using a finite differences continuous code /Barthélémy et al, 1993/. We then compute the drawdowns due to the LPT2 test, assuming that the density field is not influenced by the test.

These drawdowns are identical to the ones computed without density effects. We thus conclude that for the study of the LPT2 test, density effects due to the heterogeneous salinities may be neglected.

We also test the influence of our "skin effect" assumption upon optimization results. We use specifications identical to optimization n° 4, but the channels in contact with the sea are treated in the same way as other channels. Figure 3-4 shows the optimized transmissivities, together with the ones obtained by optimization n° 4, for reference. The new transmissivities are a little lower than the previous ones, except for NNW1, which is only indirectly affected by the supression of the "skin efect", since it is not in contact with the sea. The ratio between "skin" and "uniform zones" transmissivities varies from 0.9 (for NNW1) to 2. This is within the variations from one optimization to the other. The quadratic error S we obtain is 2.87, to be compared with S = 2.83 for optimization 4. Finally, table 3-5 shows inflows in borehole KAS06. In the "uniform zones" model, about 8 % of the flow is transferred from zone EW5 to zone NNW1, the flowrate from NNW2 being unaffected. This is simply due to the inverse variation in their transmissivities (decrease in EW5 and increase in NNW1).

Table 3-5. Inflow rates, in percent.

Optimization	EW3	EW5	NNW2	NNW1
with "skin effect"	0.05	42.5	37.35	20.1
with uniform zones	0.03	34.3	37.9	27.7
measured	16	34	28	22

We can conclude from the above results that the way we account for surface exchanges has a limited impact on the optimization results : identical quadratic errors, comparable resulting transmissivities, and moderately perturbated inflows indicate that the model is robust with respect to this type of assumption.

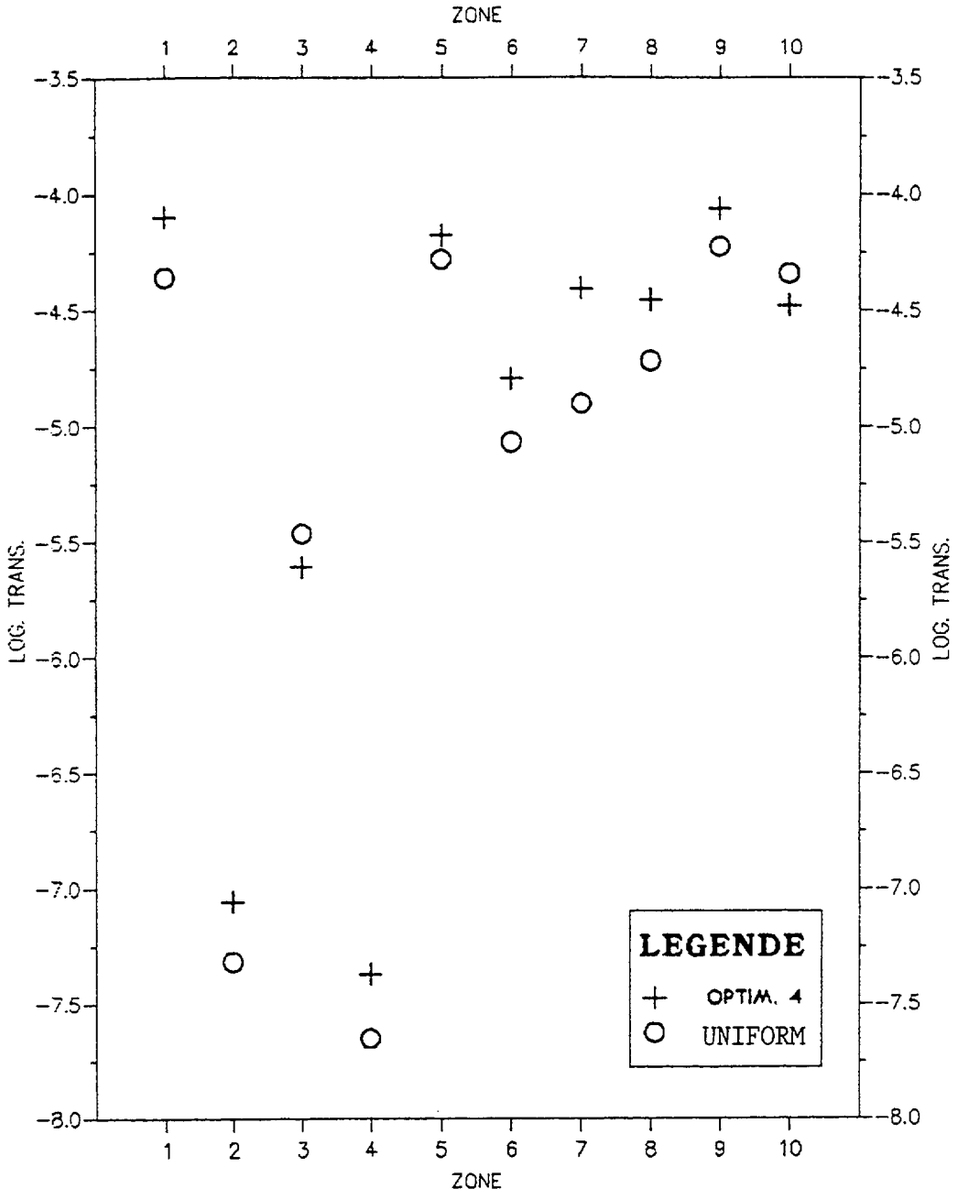

Optimized zones :

1/ EW1a	**4/ EW3**	**7/ NE1b**	**10/NNW1**
2/ EW1b	**5/ EW5**	**8/ NE2**	
3/ EW1c	**6/ NE1a**	**9/ NW1**	

Figure 3-4. Optimized transmissivities, uniform zones and "skin effect" zones.

Using a simple optimization procedure applied on the drawdowns observed at the end of the LPT2 test, we are able to constrain, within one order of magnitude, the transmissivity of most of the fracture zones we study. This is true only for the set of assumptions we work with, but the robustness of the results has been checked for salinity effects and uncertainty on sea-fracture zones exchanges. A few difficult points remain : two fracture zones, EW3 and NE2, are not well characterised ; a few observed drawdowns are poorly simulated ; the inflow from zone EW3 into the pumping borehole is not simulated. The behavior of EW3 and NE2 shows that even zones situated close to a largescale pumping test may not be influenced in a way that would enable the assessment of their hydraulic properties. In order to gain a non-ambiguous knowledge of the large scale conductors on a site such as Äspö, two or three pumping tests such as LPT2 would probably be necessary.

4 TRANSIENT SIMULATION OF LPT2

In this chapter, we simulate the evolution of drawdowns during the 92-days pumping. compared to steady-state modelling, transient-state modelling requires one more set of data : the storage behavior of the system. We do not know a priori how storage is distributed in the system. Do fracture zones account for most storage effects, or is storage more evenly distributed than flow, despite the low connectivity of the average rock ? Also, is the effect of sea-fracture zones exchanges still negligible when considering transient behavior ? We try to answer these questions, performing the following simulations of the pumping test :

- Network obtained by optimization 4. Storage is concentrated in fracture zones.
- Network obtained by the "uniform zones" optimization. Storage is still concentrated in fracture zones.
- Network reproducing storage outside the fracture zones with a sparse regular grid (200 m edge) superimposed on the fracture zones network.

4.1 TAKING STORAGE INTO ACCOUNT

For a channel network with a given geometry and given channel conductances, channel volumes are computed using the "cubic law" and an arbitrary shape factor α.

α is defined as the ratio between channel length L and channel width l :

$$L = \alpha l$$

We suppose that this ratio is the same for all channels in the network.

We then compute the total volume V_c of all channels in the model. We chose a global specific storage S_{sg} for the whole model. Knowing the size of the region we represent, we can compute the total storage S_t in the model and then the uniform specific storage s_s needed to obtain this total storage :

$$s_s = S_t / V_c$$

The storage we assign to a channel is then the product of its volume by this specific storage.

Note that here the shape factor is only an arbitrary intermediate value which has no effect on the storage assigned to each channel. Changing α would change all the channel volumes by the same ratio, thus changing s_s by the inverse of this ratio and would yield the same storage coefficients in all channels.

4.2 SIMULATIONS WITH STORAGE IN FRACTURE ZONES ONLY

We test two values of the global specific storage S_{sg} : $5.10^{-8}m^{-1}$ and $10^{-7}m^{-1}$. Figures 4-1 to 4-4 show drawdowns obtained for these two hypotheses with the network from optimization 4 ("skin effect" simulation). Figures 4-5 to 4-8 show results obtained with the "uniform zones" network. In each case, we show measured and computed drawdowns in eight borehole sections : KAS02 B4, KAS05 E3 and KAS07 J4 intersept zone EW5 ; KAS12 DC and KAS04 DI intersept zone NE2 ; KAS07 J6 intersepts NNW1 ; KAS08 M3 and KAS08 M1 intersept NNW2.

For all simulations, steady state is reached after about 10 days of pumping. We note that doubling the storage capacity of the system has no influence on its response after 10 days of pumping. The responses measured in the 10 days-92 days period are much less regular. Most drawdowns start increasing again after the effect of the flowrate change has dissipated. This increase in drawdown can take place anywhere between two days (EW5, KAS05 E3) and two months (NNW2-KAS08 M3). One notable exception is section KAS07 J6 (NNW1). Its behavior is hard to understand and is in fact poorly reproduced by simulations. Generally speaking, the measurements show that steady-state is definitely not achieved after 10 days of pumping, and maybe not even after 92 days.

The shape of the drawdown curves for the first three days of pumping is generally well reproduced. If we drastically increase storage to reproduce the increase of drawdowns between 10 days and 92 days, this will also delay the start of the response, which is not justified. In fact, the lower of the two storages we test gives better early-time (0 to 3 days) responses.

The "skin effect" and "uniform zones" models give practically identical results. If the early steady-state we find in our simulations was due to the proximity between imposed heads (at contact between fracture zones and the sea) and the pumping borehole, adding or removing the "skin effect" would have a major impact on this part of the drawdown curves. This is not the case.

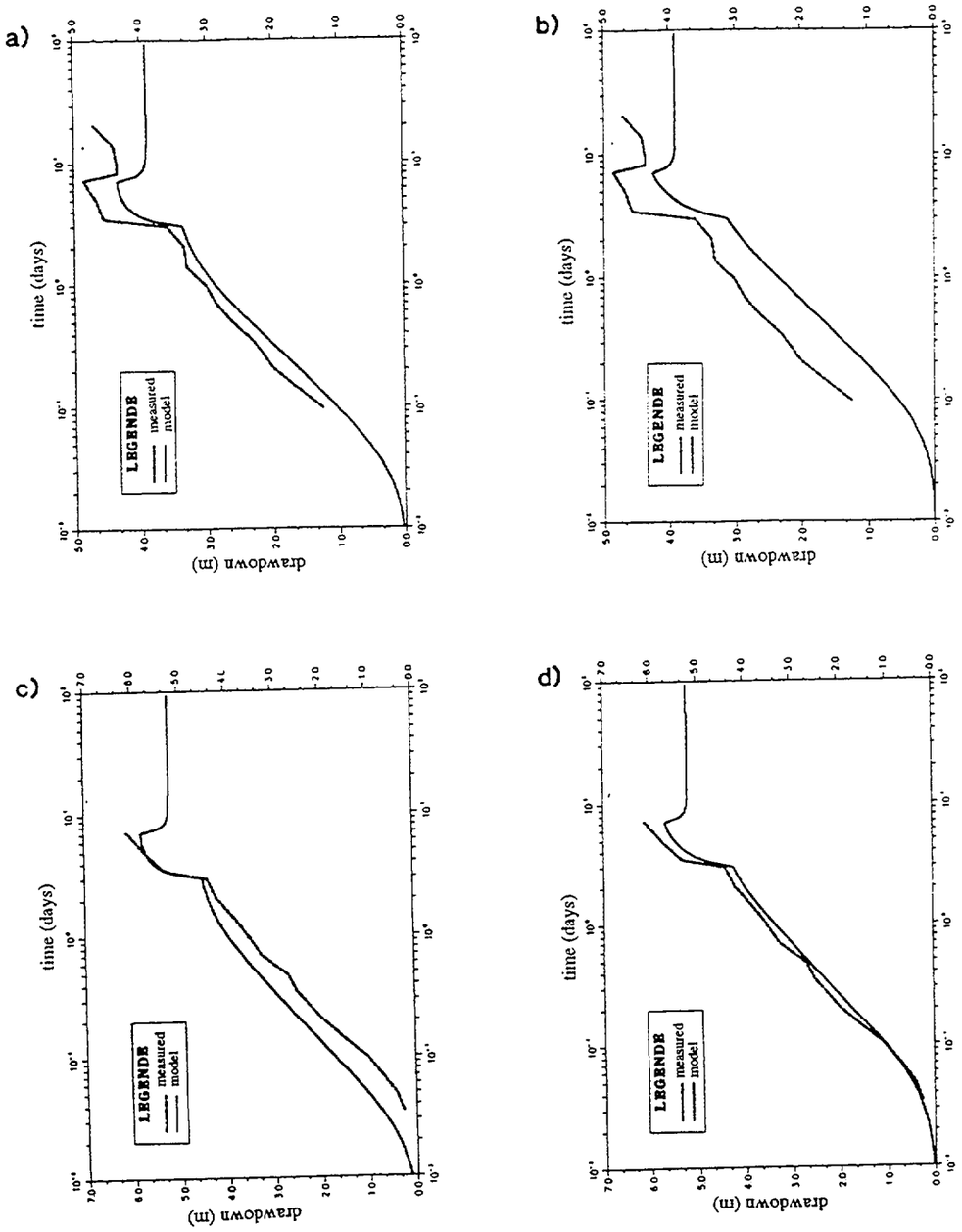

Figure 4-1. Drawdown versus time, "skin effect" network section KAS05 E3, zone EW5 : a) $S_{sg} = 5.10^{-8}$ m^{-1} . b) $S_{sg} = 10^{-7}$ m^{-1} section KAS02 B4, zone EW5 : c) $S_{sg} = 5.10^{-8}$ m^{-1} . d) $S_{sg} = 10^{-7}$ m^{-1}.

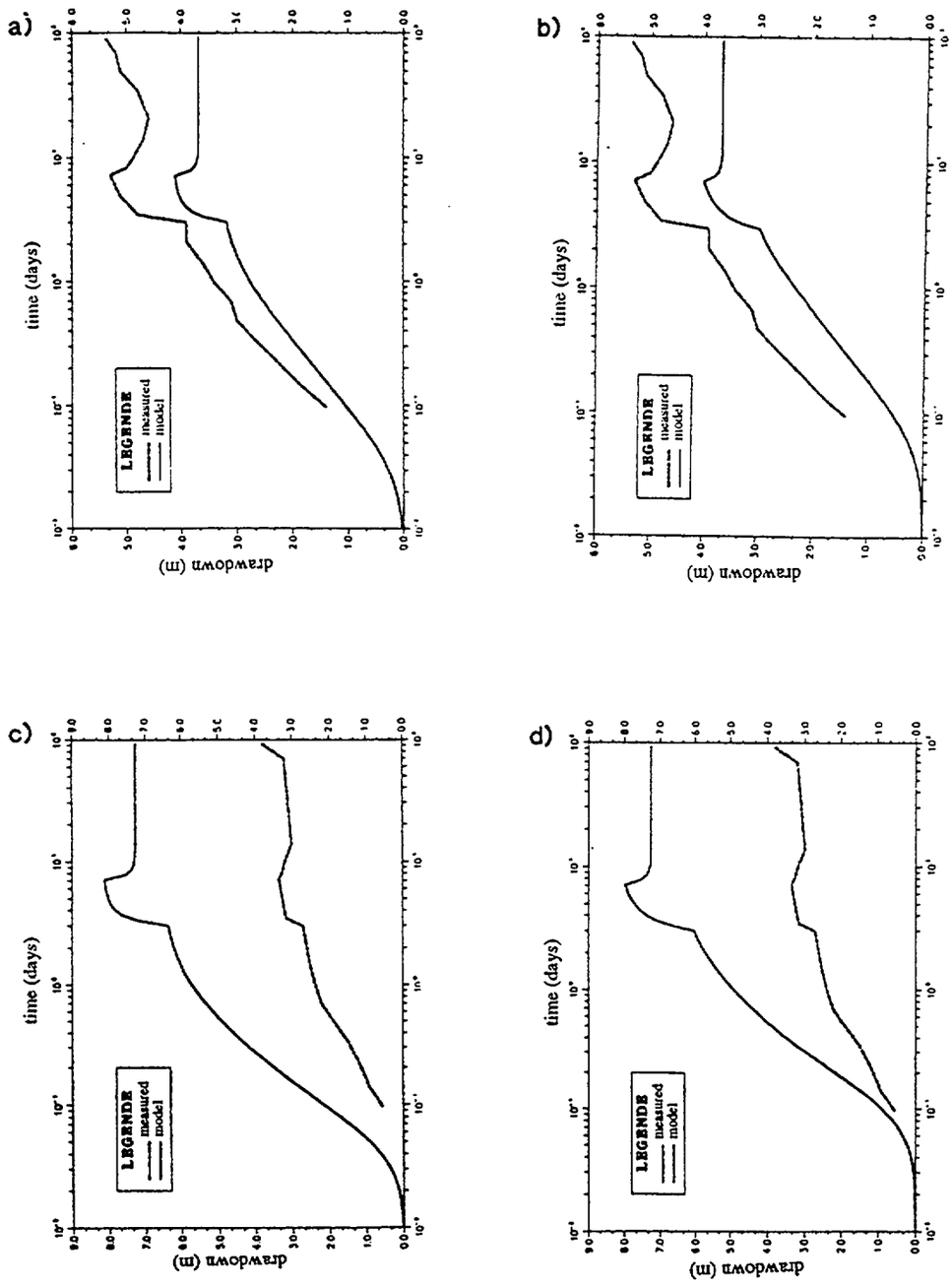

Figure 4-2. Drawdown versus time, "skin effect" network section KAS07 J4, zone EW5 : a) $S_{sg} = 5.10^{-8}$ m^{-1} . b) $S_{sg} = 10^{-7}$ m^{-1} section KAS08 M1, zone NNW2 : c) $S_{sg} = 5.10^{-8}$ m^{-1} . d) $S_{sg} = 10^{-7}$ m^{-1}.

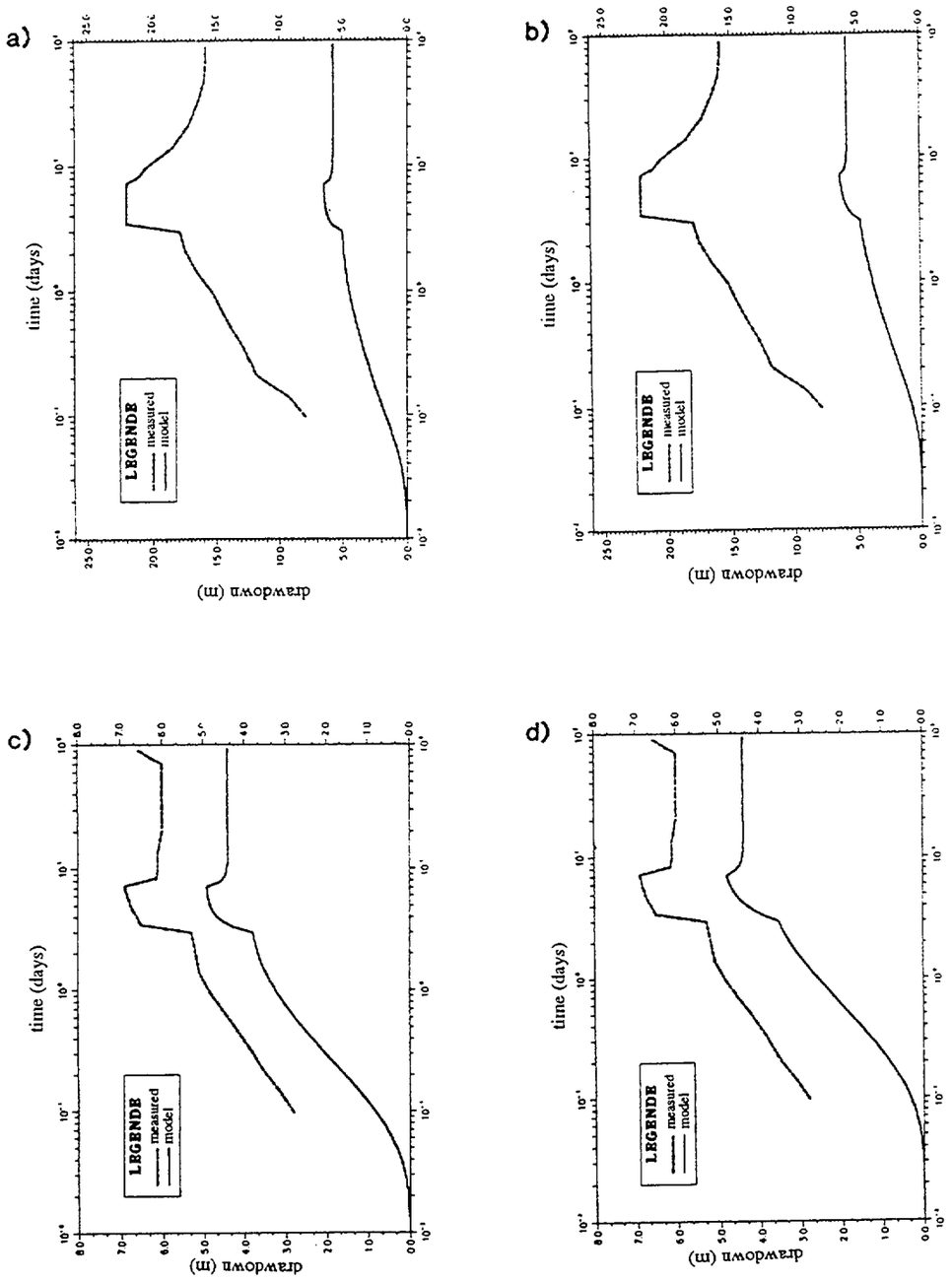

Figure 4-3. Drawdown versus time, "skin effect" network section KAS07 J6, zone NNW1 : a) $S_{sg} = 5.10^{-8}$ m^{-1} . b) $S_{sg} = 10^{-7}$ m^{-1} section KAS08 M3, zone NNW2 : c) $S_{sg} = 5.10^{-8}$ m^{-1} . d) $S_{sg} = 10^{-7}$ m^{-1}.

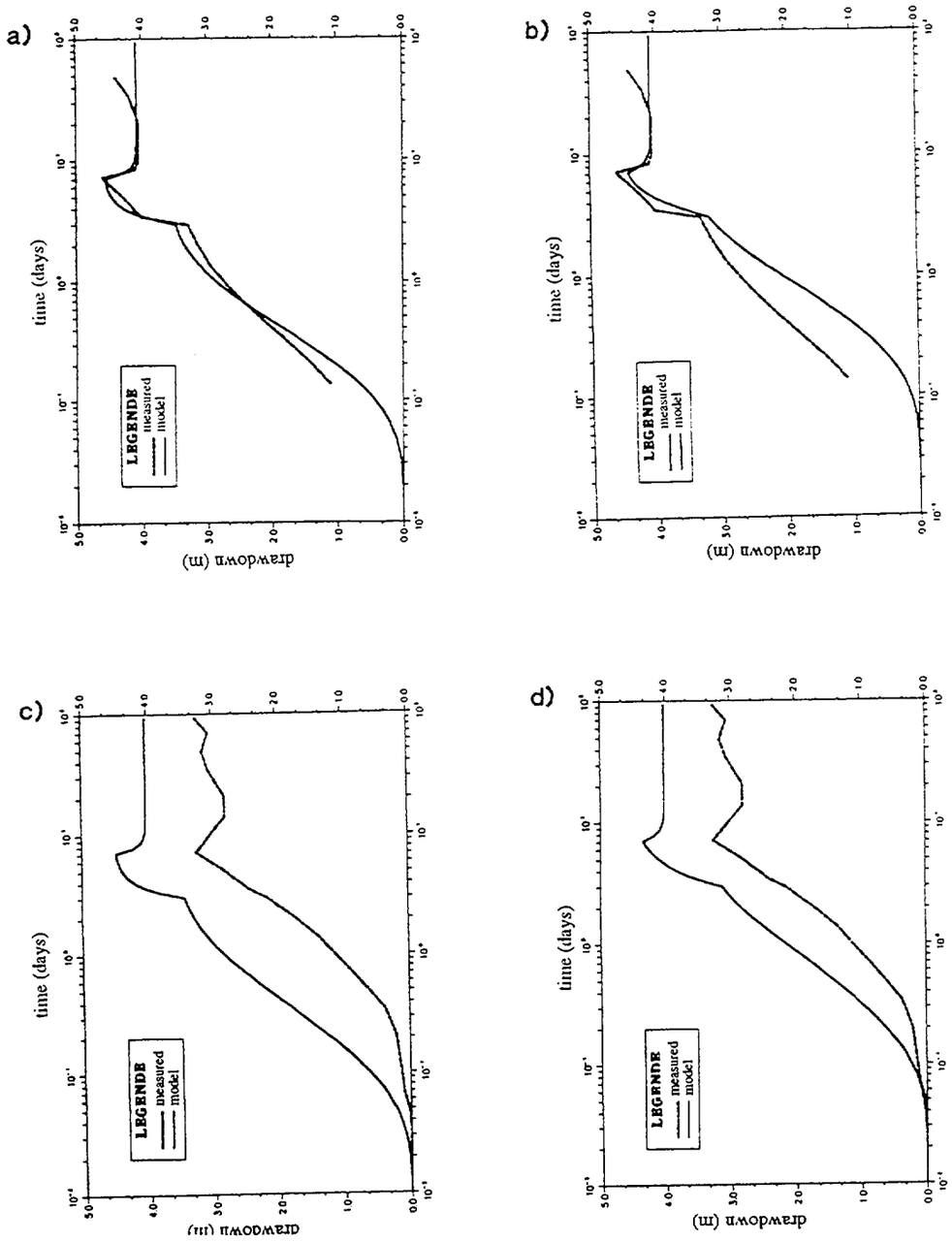

Figure 4-4. Drawdown versus time, "skin effect" network section KAS12 DC, zone NE2 : a) $S_{sg} = 5.10^{-8}$ m^{-1} . b) $S_{sg} = 10^{-7}$ m^{-1} section KAS04 D1, zone NE2 : c) $S_{sg} = 5.10^{-8}$ m^{-1} . d) $S_{sg} = 10^{-7}$ m^{-1}.

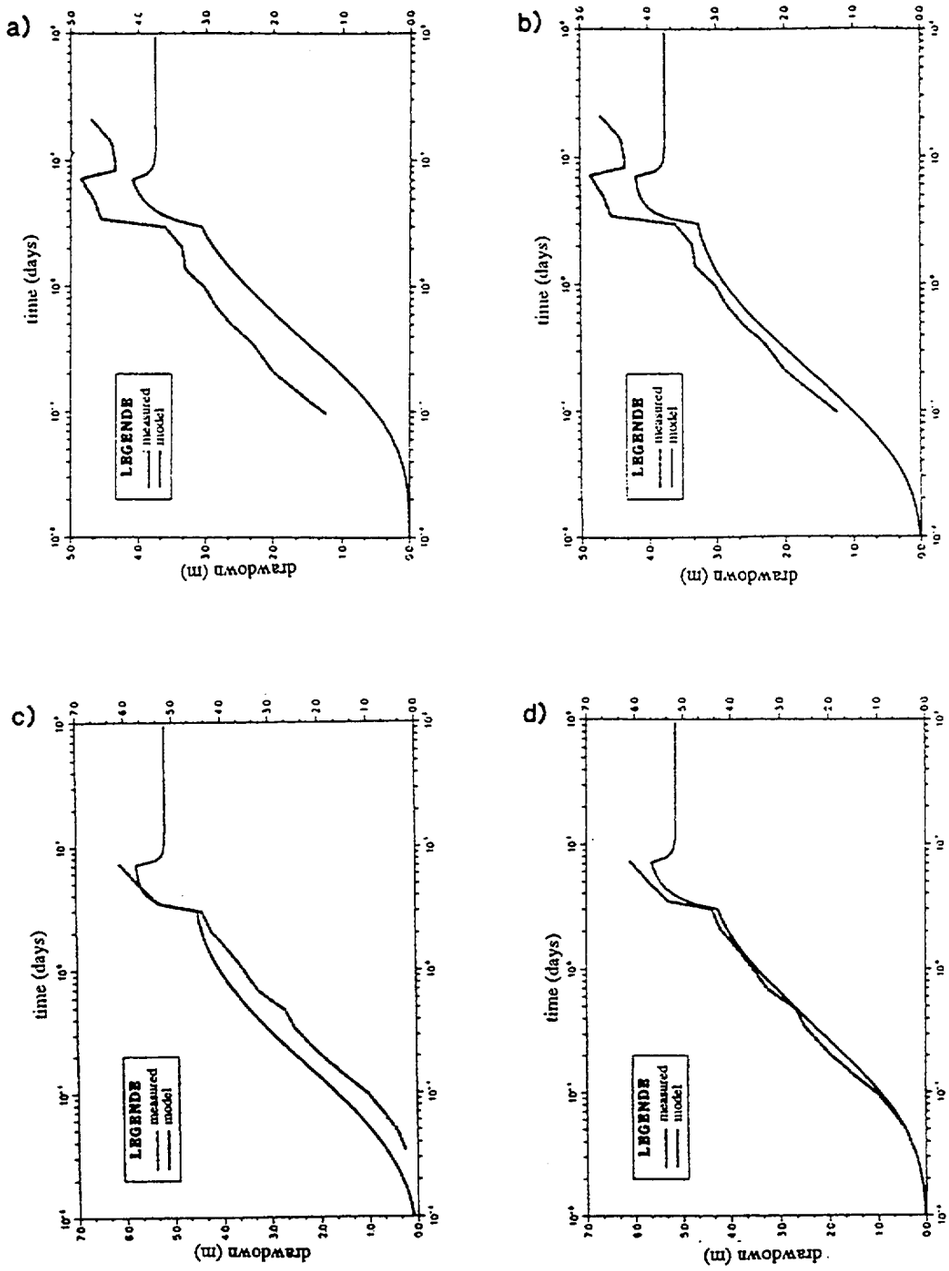

Figure 4-5. Drawdown versus time, "uniform zones" network section KAS05 E3, zone EW5 : a) S_{sg} = 5.10^{-8} m^{-1} . b) S_{sg} = 10^{-7} m^{-1} section KAS02 B4, zone EW5 : c) S_{sg} = 5.10^{-8} m^{-1} . d) S_{sg} = 10^{-7} m^{-1}.

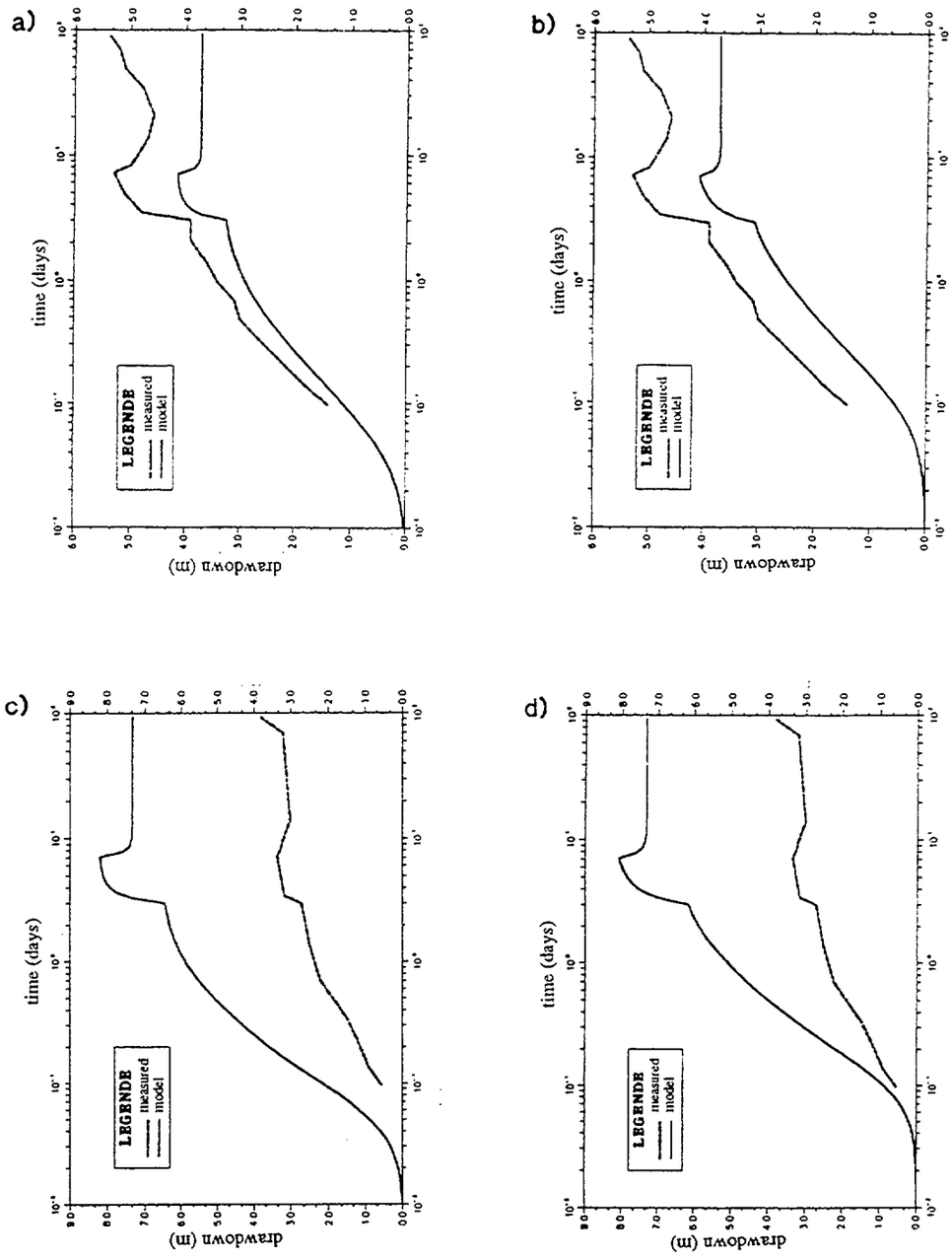

Figure 4-6. Drawdown versus time, "uniform zones" network section KAS07 J4, zone EW5 : a) $S_{sg} = 5.10^{-8}$ m^{-1} . b) $S_{sg} = 10^{-7}$ m^{-1} section KAS08 M1, zone NNW2 : c) $S_{sg} = 5.10^{-8}$ m^{-1} . d) $S_{sg} = 10^{-7}$ m^{-1}.

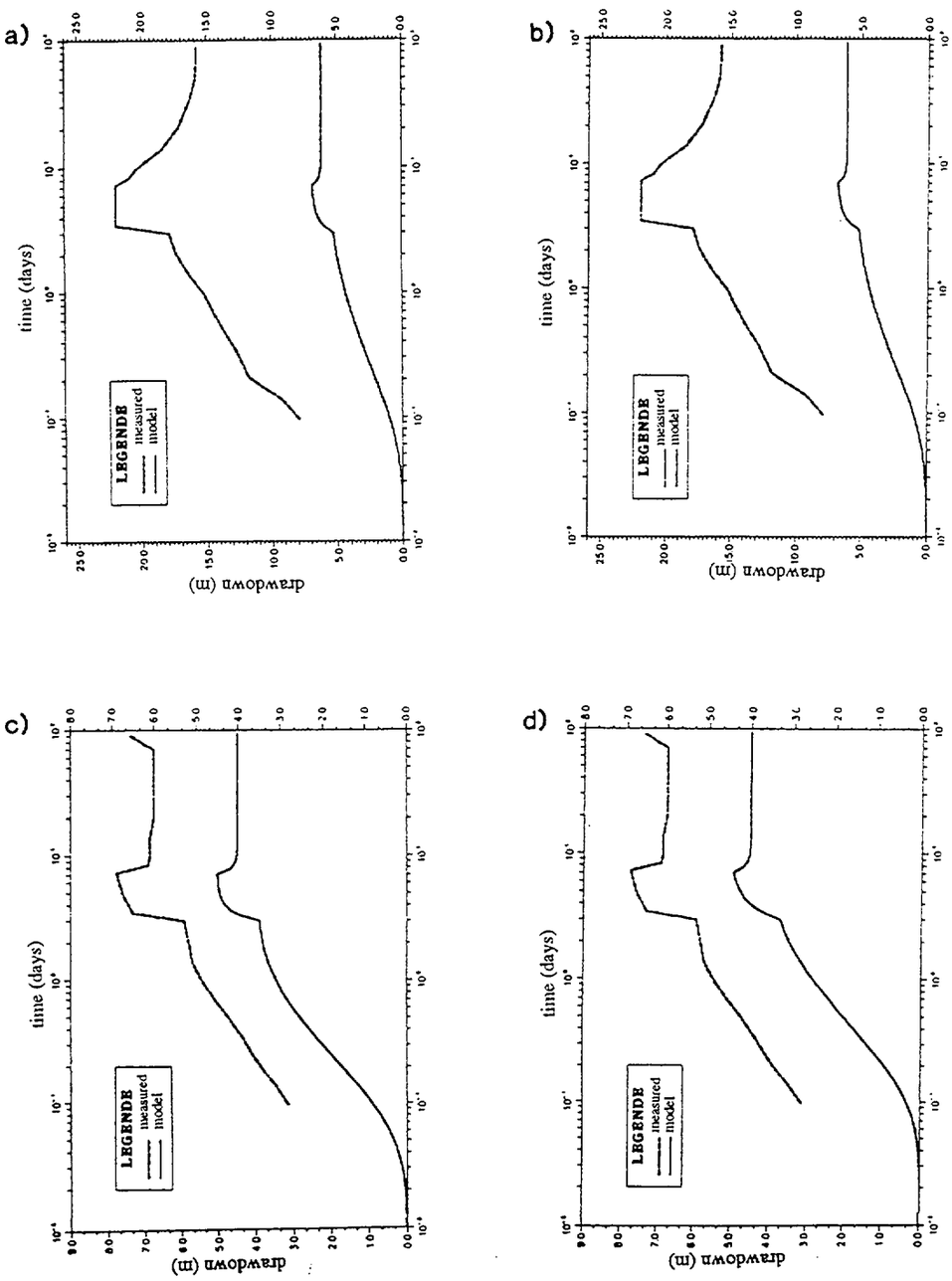

Figure 4-7. Drawdown versus time, "uniform zones" network section KAS07 J6, zone NNW1 : a) $S_{sg} = 5.10^{-8}$ m^{-1} . b) $S_{sg} = 10^{-7}$ m^{-1} section KAS08 M3, zone NNW2 : c) $S_{sg} = 5.10^{-8}$ m^{-1} . d) $S_{sg} = 10^{-7}$ m^{-1}.

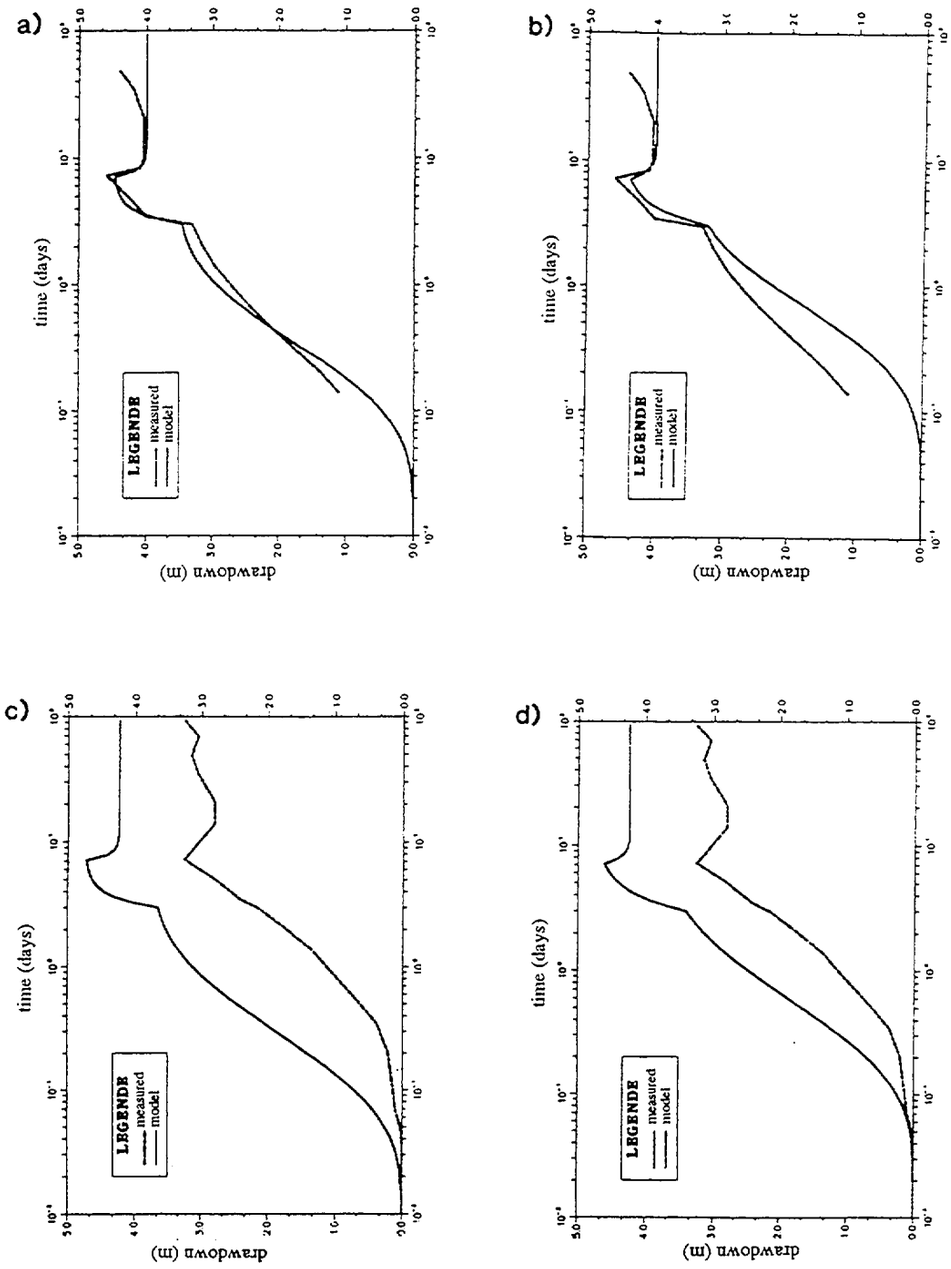

Figure 4-8. Drawdown versus time, "uniform zones" network section KAS12 DC, zone NE2 : a) $S_{sg} = 5.10^{-8}$ m^{-1} . b) $S_{sg} = 10^{-7}$ m^{-1} section KAS04 D1, zone NE2 : c) $S_{sg} = 5.10^{-8}$ m^{-1} . d) $S_{sg} = 10^{-7}$ m^{-1}.

In order to reproduce the later part of the response, we need to take into account the distribution of storage between fracture zones and the average rock. Paragraph 4-3 describes such an attempt.

4.3 SIMULATIONS WITH STORAGE IN ROCK MATRIX

In order to reproduce storage effects outside fracture zones, we use the following method :

- First, generate the 22 fracture zones without any change.
- Add horizontal and vertical "pseudo-zones". These zones are oriented along the three planes of coordinates. They are spaced 200 m along x (east) and y (north), and 100 m along z (vertical).
- Define the channel density in "pseudo-zones" as zero. In this way, only the intersections of these zones with each other and with the 22 real fracture zones will define channels : a regular 200 m x 200 m x 100 m grid is superimposed to the fracture zones channel network. Note that we also add channels in each fracture zone, where it is intersected by pseudo-zones. Figure 4-9 shows the whole model, while figure 4-10 shows zone NE2 before and after superimposing the regular grid : a new, non orthogonal sparse grid is added to the 25 m-edge channel grid.

Boundary conditions are unchanged : no flow on bottom face, zero imposed head on lateral faces, mixed condition on top face. We suppose that surface exchanges are limited to fracture zones. Therefore the superimposed regular grid is not connected to the surface outside fracture zones.

We assign to each element of the regular grid a conductance of 5.10^{-4} m^3/s. At a large enough scale, such a grid would have an equivalent permeability Keq = 2.5 10^{-8} m/s. In fact, this grid is far from being equivalent to a porous medium, since the scale of interest here (size of the model blocks between fracture zones) is a few hundreds of meters, while this grid has a Representative Elementary Volume (REV) on the order of 2 km (10 grid cells).

Therefore, the regular grid acts as a network of discrete conductors linking fracture zones, and more importantly as a "reservoir", since we assign to this grid 90 % of the total storage S_t in the model, while fracture zones account for 10 % of S_t. Storage in each channel is then computed as previously.

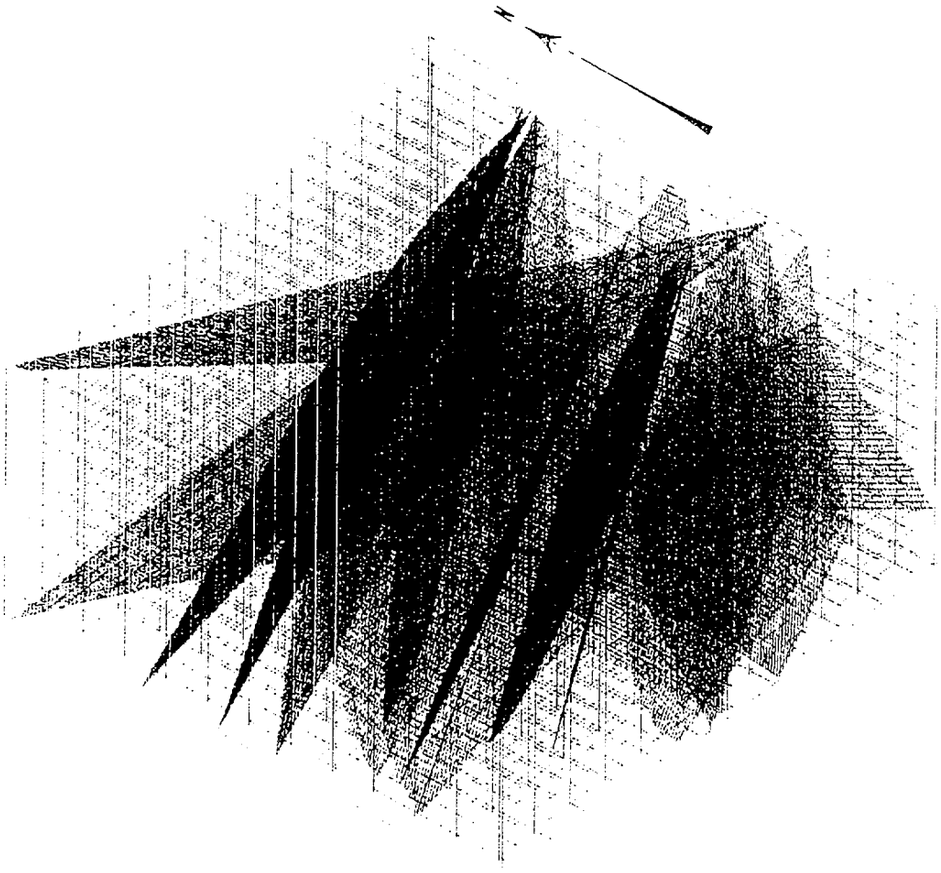

Figure 4-9. Model with superimposed grid-general view.

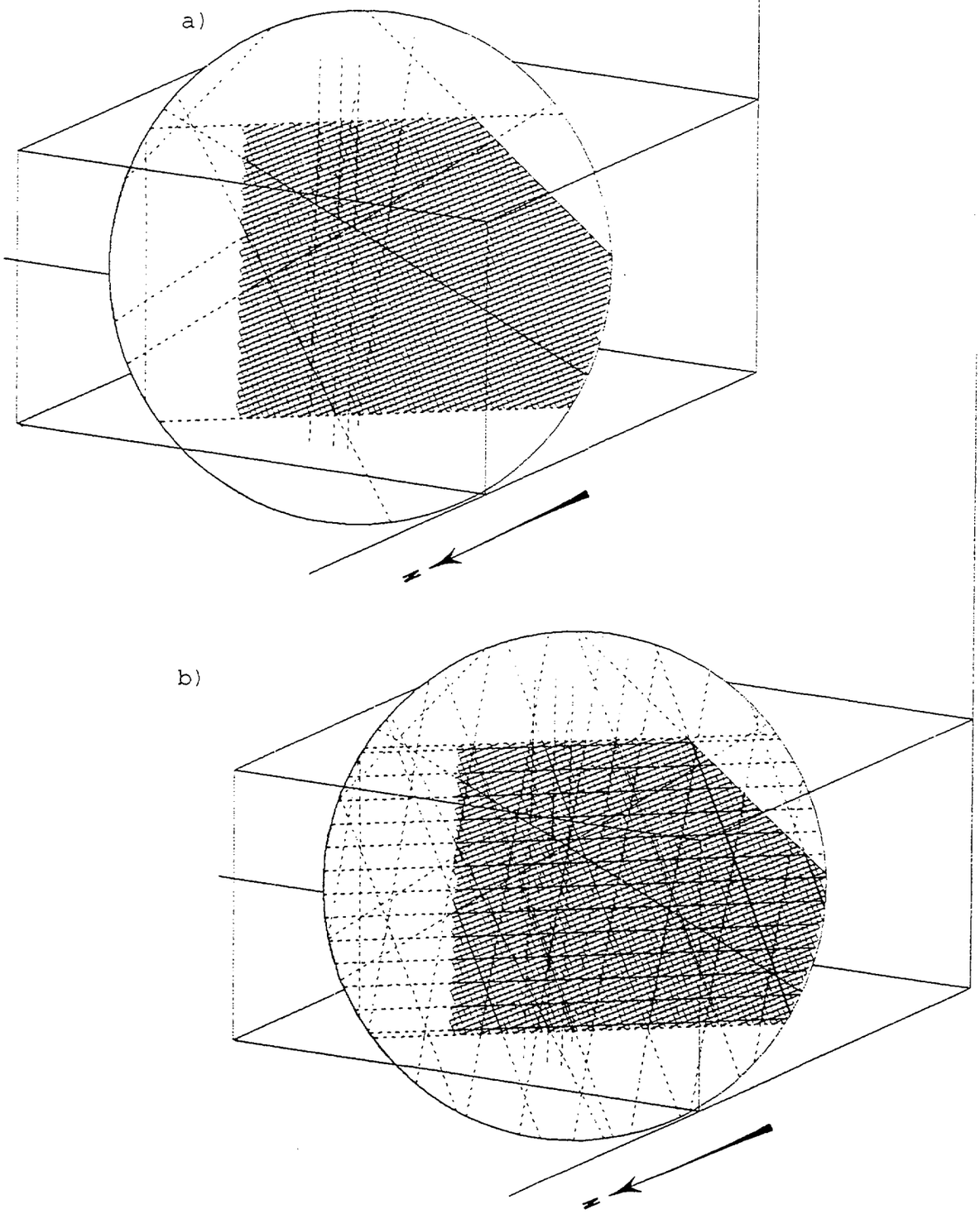

Figure 4-10. Channels in zone NE2
a) fracture zones only,
b) with superimposed grid.

The total storage in the model is the same as the one obtained for $S_{sg} = 10^{-7}$ m^{-1} in the previous simulations. Because we are adding channels to the network not only between the fracture zones, but also inside the zones, we cannot use directly the conductances we obtained from fracture-zone-only optimizations. This would increase the overall transmissivity of the zones, while adding a supplementary network of conductors, thus introducing a bias. We therefore first perform a steady-state optimization, with the same parameters as for optimization 4. The same 10 zones as before are studied, conductances remaining constant for channels in the other 12 zones, as well as for channels outside the zones. Table 4-1 shows the results of this optimization, and compares them with results from optimization 4.

Channel conductances go down in 6 zones out of 10. Orders of magnitude do not change, except for zones EW1a and NW1. The quadratic error S is improved by 20 %, while relative inflow rates are severely degraded. This can be explained as follows. The goodness of fit for the model with fracture zones only is limited by the fact that flow in the model is bound to be regular (identical channel conductances and square grid in each zone) while real flow is not regularly distributed, as shown by large drawdown differences between close observation points. Adding the "out of zones" network, with channel conductances close to the ones in the zones, but a spacing eight times larger, introduces irregularities in the flow pattern.

Table 4-1. Optimization results with and without superimposed grid.

a)

zone	Channel conductance (m^3/s) optimization 4 (chap.3)	Channel conductance (m^3/s) optimization with regular grid
EW1a	$2.00\ 10^{-3}$	$1.25\ 10^{-5}$
EW1b	$2.20\ 10^{-6}$	$1.24\ 10^{-5}$
EW1c	$6.18\ 10^{-5}$	$1.41\ 10^{-4}$
EW3	$1.06\ 10^{-6}$	$2.72\ 10^{-7}$
EW5	$1.67\ 10^{-3}$	$3.00\ 10^{-4}$
NE1a	$4.01\ 10^{-4}$	$1.51\ 10^{-3}$
NE1b	$9.81\ 10^{-4}$	$6.31\ 10^{-4}$
NE2	$8.81\ 10^{-4}$	$5.90\ 10^{-4}$
NW1	$2.18\ 10^{-3}$	$7.49\ 10^{-5}$
NNW1	$8.31\ 10^{-4}$	$1.47\ 10^{-3}$
final optimization quadratic error (m^2)	2.83	2.20

b)

zone	Inflow rates in percent	
EW3	0.05	0.02
EW5	42.5	9.60
NNW2	37.35	45.50
NNW1	20.11	44.90

More important local head variations can be obtained. Optimization will then adapt these irregularities to the measured ones. However, one extra channel close to the intersection between a fracture zone and the pumping borehole is enough to seriously offset the inflow rates balance.

Figures 4-11 and 4-12 show drawdowns obtained for the eight observation sections discussed previously. Responses during the first three days are close to the ones simulated with fracture zones only and with $S_{sg} = 10^{-7}$ m^{-1}, and are generally slightly delayed. After 10 days of pumping, drawdowns start increasing again in all the observation sections we study. It seems that the distribution of storage between fracture zones and "average rock" is effectively the key factor for reproducing correctly both the short term and the long term behaviors during the test.

4.4 CONCLUSION

Transient-state simulations of LPT2 have brought more information on several points. First, the similarity between "uniform zones" and "skin effect" simulations confirms that our model is robust with respect to exchanges between the sea and fracture zones. Taking into account only fracture zones, we are able to reproduce correctly the response of the system during the first ten days. In order to reproduce the evolution of drawdowns at later times, we need to take into account the storage effect of average rock. We chose to superimpose a sparse regular grid over the fracture zones channel network to represent the average rock storage. This choice is consistent with the findings of the connectivity study (paragraph 2.2), which concludes that fractures are connected, but that the Representative Elementary Volume for equivalence with a porous medium is larger than the scale of interest.

Adding this new network we need two extra parameters : the conductance of the channels (we suppose thes conductance is uniform), and the distribution of storage between this network and the fracture zones network. Simulations using one pair of parameters show responses close to measured values.

Using such superimposed channel networks is a promising method : it correctly reproduces hydrodynamic phenomena, while freeing us from the equivalent continuum assumption, which is hardly acceptable in sites such as Äspö.

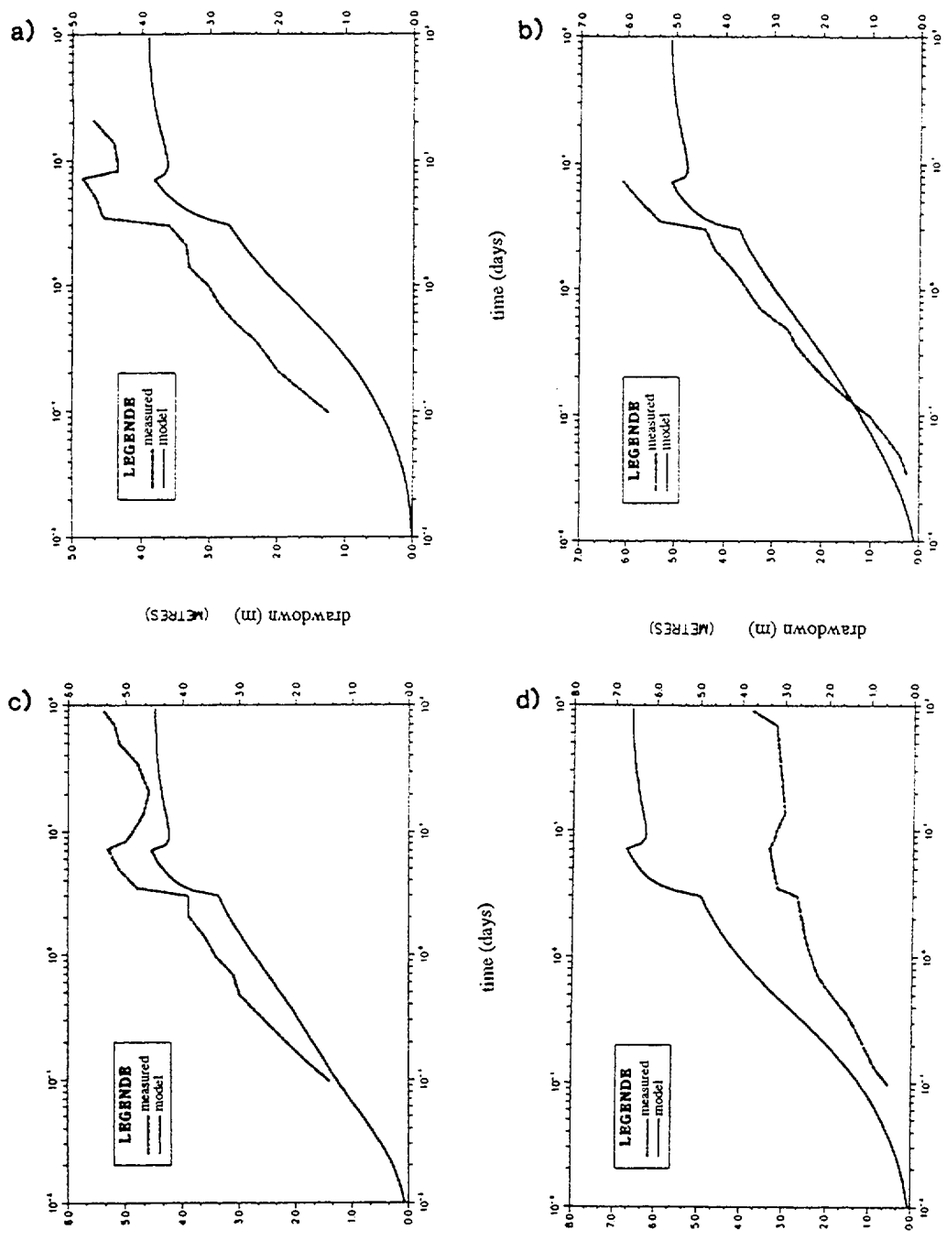

Figure 4-11. Drawdown versus time, model with superimposed grid.
a) section KAS05 E3, zone EW5
b) section KAS02 B4, zone EW5
c) section KAS07 J4, zone EW5
d) section KAS08 M1, zone NNW2

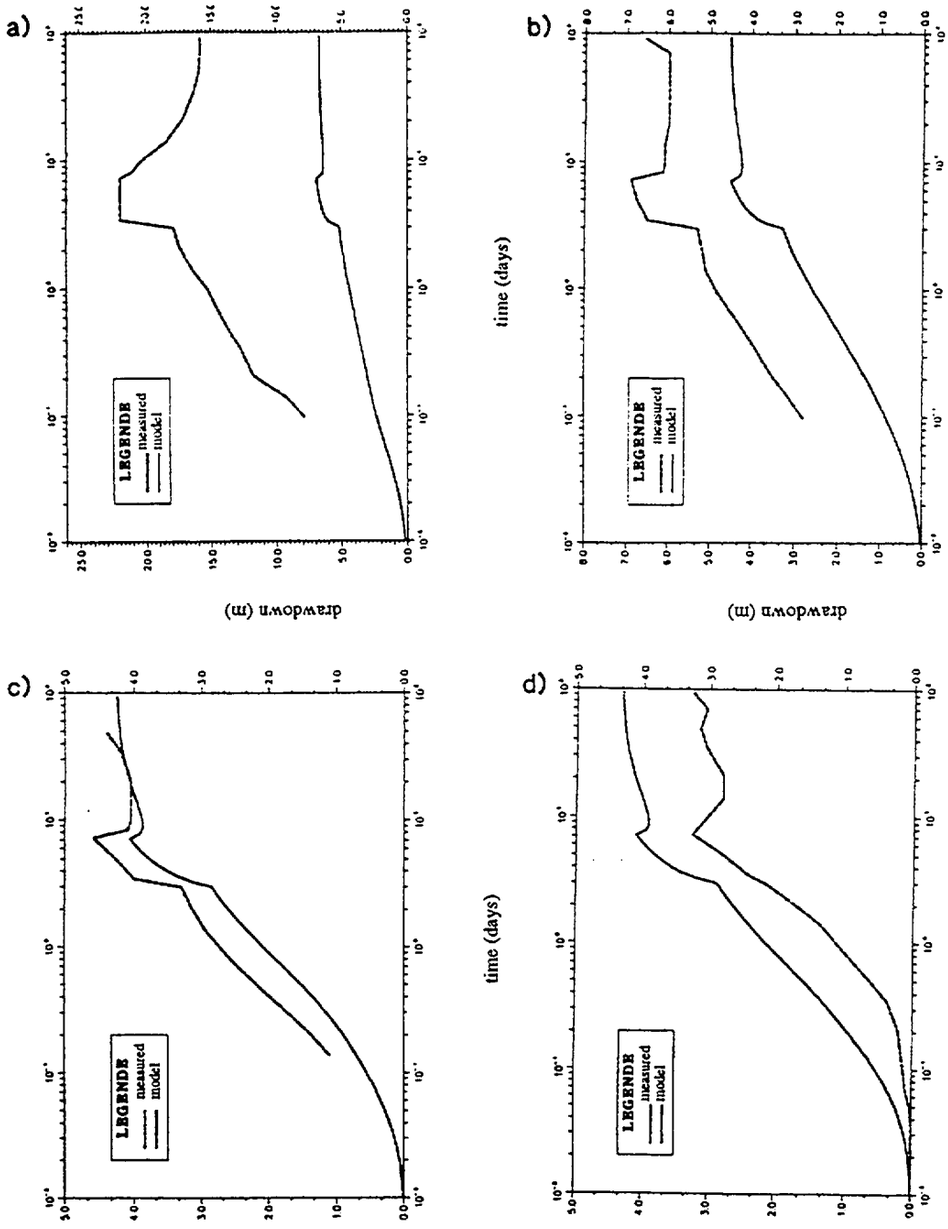

Figure 4-12. Drawdown versus time, model with superimposed grid.
a) section KAS07 J6, zone NNW1
b) section KAS08 M3, zone NNW2
c) section KAS12 DC, zone NE2
d) section KAS04 D1, zone NE2

5 PRELIMINARY SIMULATION OF A TRACER TEST

Transport simulations for this project are restrained to a feasibility study. The objective here is to assess the suitability of the flow model for reproducing realistic tracer breakthroughs in the pumping borehole. We choose to study the injection of Rhenium 186 in borehole section KAS08-M1 (fracture zone NNW2). We use the programme TRIPAR to model tracer transport. This code uses the particle-tracking method to simulate adjective-dispersive transport in interconnected networks of one - dimensional channels.

This code has been modified to take into account radioactive decay, since the Rhe 186 half-life is 3.8 days.

Seven successive injections were performed, over a 620 hours period. Masses of injected tracer are taken from report SKB TR 92-32, appendix C, table 3-6. Masses of collected tracer used for comparison with simulation results are taken from the same appendix, figure 4-8. According to this report, the mass of tracer collected corresponds to a 30.4 % recovery (after correcting for radioactive decay). The flow regime in our model imposes a 100 % simulated recovery rate. We thus cannot reproduce tracer losses. In order to overcome this problem, we use a classical but not satisfying fix : at each injection step, the mass of tracer injected in the model is taken as the real injected mass times the recovery rate.

The flow system we use is the one resulting from optimization 4. We assume a steady-state, considering that the bias we introduce in our computations can be negleted for a simulation of limited scope (feasability study only). In order to reproduce arrival times similar to the measured ones (about 100 hours), we use a shape factor $\alpha = 8.10^{-2}$. For ideal ribbon-shaped channels with uniform thickness and width, this would correspond to channel widths equal to twelve times channel lengths. In fact, channels are highly heterogeneous features. For a given mean channel conductance, heterogeneity (i.e. constrictions, dead-end volumes, etc...) results in a drastic decrease of the mean flow velocity. Since the mean velocity we compute for a channel with a given conductance increases when its shape factor increases, irregular channels result in a low apparent shape factor. The shape factor we use here therefore corresponds to fairly heterogeneous channels.

Figure 5-1 shows the total mass flux in the pumping borehole obtained using a longitudinal dispersivity of 6.5m in channels.

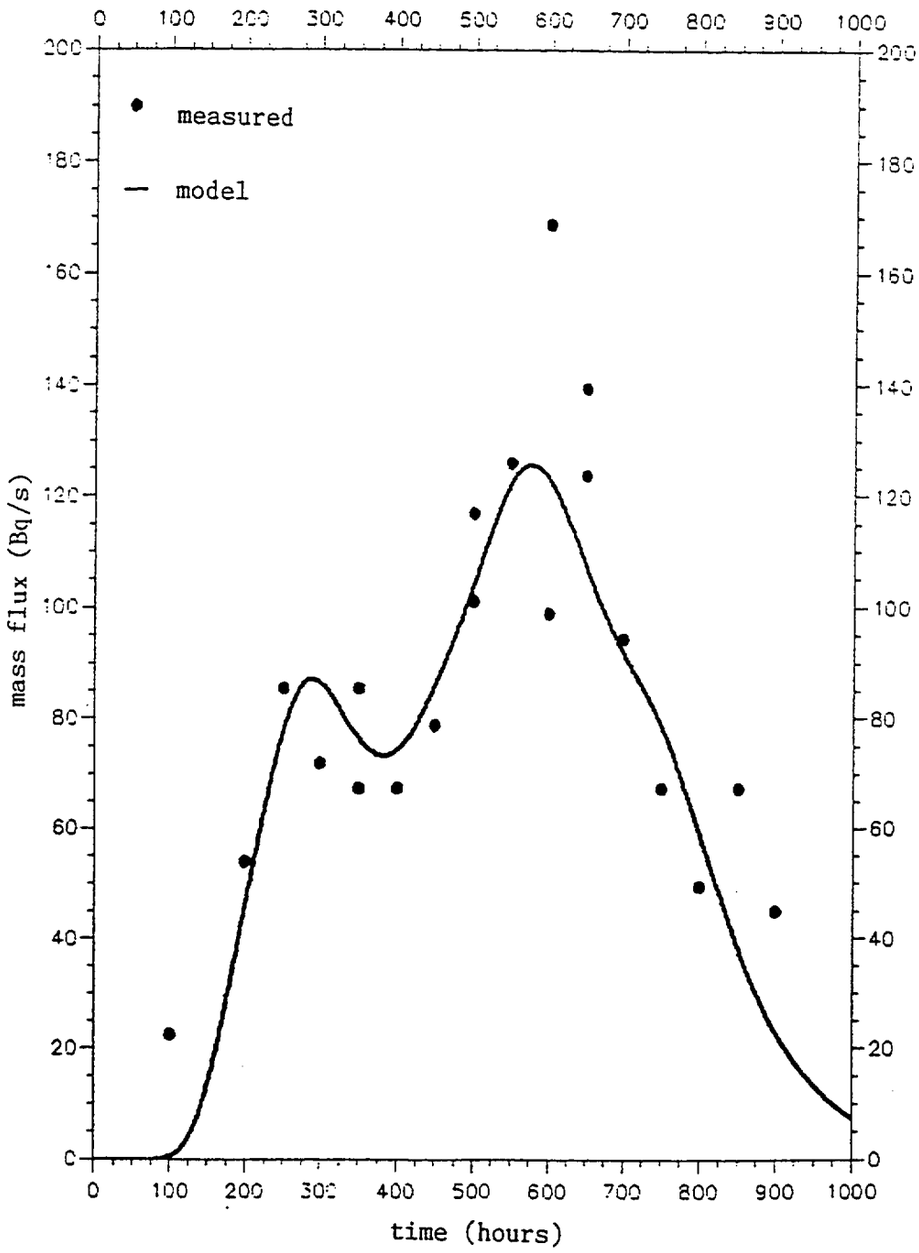

Figure 5-1. Breakthrough curve for Rhenium 186.

The breakthrough curve correctly reproduces the observed behavior. Note that the last two measurement points in the figure probably correspond to the arrival of Rhe 186 injected in borehole section KAS08 M3 starting 677 hours after the start of the KAS08 M1 injection. This explains why the two points are way above the computed curve.

Figure 5-2 shows tracer trajectories in the model. Every channel which was visited at least once by a particle during the simulation is represented. Because of the important longitudinal dispersion in channels, a particle can effectively go back upstream, especially if it is in a slowly flowing channel. This explains the "dead-ends" we notice on the figure. Advection-only simulations produce "visited channels" maps without dead-ends.

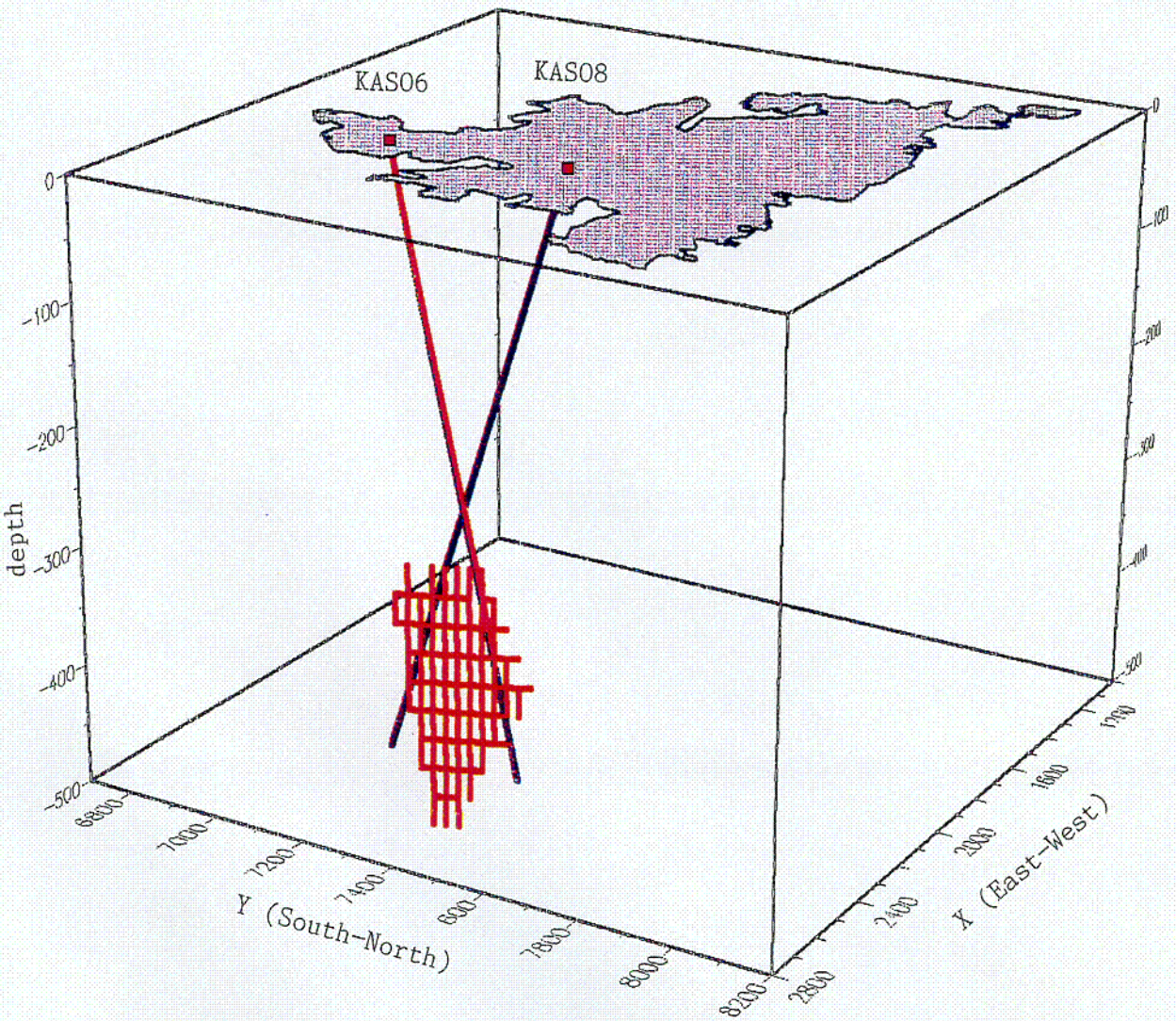

Figure 5-2. Channels visited by the tracer.

C-04

Transport occurs here almost exclusively in zone NNW2, and the injection in the KAS08 M1 section does not influence zone NE1a. Although the plane supporting this zone intersects the borehole, the zone itself is restricted in our model to the south side of its intersection with the south-dipping EW3, and is therefore not hydraulically active near the intersection between its plane and KAS08.

To conclude on this feasability study, the model we use is able to correctly reproduce a tracer breakthrough curve, provided we use a shape factor corresponding to a strong heterogeneity in each channel. However, we do not simulate tracer losses.

6 CONCLUSION

The main results we have obtained are reviewed. They are then situated in the perspective of discrete fracture models development.

6.1 RESULTS

The geometry of the fractured medium was first defined more precisely, considering both fracture zones and the average rock. Connections between fracture zones, and between boreholes and fracture zones were checked and compared with our assumption on fracture zone extensions at depth. Also, using fracture traces mapped in the laboratory access drift, we evaluated the connectivity of the fracture field outside fracture zones. The "average rock" fractures can be classified as above the percolation threshold, therefore flow paths through the average rock may exist at any scale. However, these flow paths are very sparse, so that assimilating such a network to a continuous medium would not be rigorous at the scale of interest. Since fracture zones are largely predominant, most of our simulations do not take average rock into account.

A simple procedure for optimizing fracture zone transmissivities was adapted to our software. This method minimises the sum of square errors between computed drawdowns and observed drawdowns. We applied it to modelling the end of the LPT2 pumping test, assuming that the end-of-pumping measurements are close to steady state. Varying weights may be assigned to the observation points where the quadratic errors are computed. We optimized the transmissivity of ten out of the twenty-two zones, using six different sets of parameters. These six optimizations give generally consistent results. Fitted fracture zone transmissivities stay within one order of magnitude for the six optimizations (except zones EW3 and NE2). It seems that a large scale pumping test such as LPT2 is therefore an efficient way of constraining the transmissivity of fracture zones at the kilometer scale we studied here.

We incorporated into our model the ability to account for water density variations due to salinity contrasts. Simulations with, and without, density variations showed that these variations may be neglected for modelling LPT2.

The nature of the contact between the Baltic Sea and the fracture zones was not known and was likely to have a strong influence on the flow regime. Two optimizations were compared, one assuming that fracture zone transmissivity does not change next to the sea, and the other assuming that fracture zone transmissivity is divided by 20 where a zone intersects the sea. These two optimizations gave similar results. Therefore the data obtained from the pumping test does not allow a discrimination between the two assumptions.

Transient simulations of the pumping test showed that storage in fracture zones explains the start (first few days) of the drawdown curves, while storage in the average rock explains the increase in drawdowns between 10 and 92 days of pumping. We have developped a simple method to reproduce, using a channel-only numerical code, the effect of average rock storage. An orthogonal regular grid is superimposed to the channel network representing fracture zones. This "percolation network"-type approach properly takes into account the discrete nature of flow. We were able to produce in this way drawdown curves close to the measured ones, except for a few notable exceptions.

A preliminary simulation of tracer transport was performed. In order to model Rhenium 186 injections, we incorporated in our model the handling of exponentially decaying tracers. By fitting a channel shape factor, we were able to reproduce the shape of the breakthrough curve. However the model could not explain tracer losses : boundary conditions impose a recovery close to 100 %, whereas the measured recovery rate is about 30 % (after taking into account radioactive decay).

6.2 UTILITY OF A DISCRETE MODEL AT SITE SCALE

Models explicity reproducing networks of fractures for the hydrodynamic analysis of fractured rock were first developed mostly in order to study the relationships between the observable geometry of fractures (density, orientation, length of traces) and the permeability tensor of an "equivalent porous medium". such studies showed that for some sites the Representative Elementary Volume (REV), smallest volume for which the continuum approximation is correct, was larger than the scale of variation of the fracture field parameters /Billaux, 1990/. Specifically, for many cristalline sites, fractures tend to be organised in "clusters", or "fracture zones", cutting through a less intensively fractured "average rock" where only a minimal part of the flow occurs.

In order to represent such systems, a first approach is to explicitely generate a fracture field with a variable density, where fracture zones are reproduced by higher density zones. Since fracture densities typically vary from 10^{-2} to 1 fracture per cubic meter in average rock, and from 1 to 15 fractures per cubic meter in fracture zones, this approach is out of reach at the site scale (kilometers). At an intermediate scale (hundred of meters), it is viable provided one eliminates systematically from the model the smallest fractures, which contribute little to flow. However eliminating small fractures is not totally satisfactory, since these fractures constitute most of the porosity and therefore have a strong influence on storage effects.

We have chosen, for simulating the Äspö island and the LPT2 test, a model as simple as possible but reproducing the main known features of that site : importance of fracture zones, and channeling. In this model, each fracture zone is represented by a two-dimensionnal regular channel grid. A three-dimensionnal regular grid may or may not be superimposed to represent the sparsely connected average rock. This approach is flexible enough to be used for parametric studies involving a large number of successive simulations. In this way, we are able to test how robust are the assumption we make. At site scale, this is particularly useful during the first phases of site investigations. At such stages, many hypotheses are still possible, and parametric studies help testing their consequences, in order to focus further investigations on the most important phenomena.

Appendix

Model and Code Specification

Name, version and origin of the code

CHANNET (CHANel NETworks), version 1.0
Code development started in Lawrence Berkeley Laboratory. Current verion finalized in BRGM and ITASCA Consultants.

General description

Set of programmes for generating disc-shaped fractures, specifying a network of one-dimensional channels supported by these fractures, and computing flow and solute transport through this network.

Conceptual and mathematical model

Flow and transport are located in channels. A channel is a simple one-dimensional "tube" linking two channel intersections. Flow in a channel obeys the Darcy law. Transport in a channel obeys the one-dimensionnal advection-dispersion equation. Full mixing is assumed at intersections. The arrangement of channels on a fracture disc may be one of three types :

. channels are thrown at random on the disc ;
. a grid of regularly-spaced channels is applied ;
. channels connect only the fracture center and the centers of its intersections with other fractures.

For the first two types, channel generation may be restricted inside a polygon-shaped region, the "active region". Also, dead-ends may or may not be eliminated.

The discs may be fully specified, or may be generated at random (Poisson distribution). In the later case, conditioning may be used to force an exact representation of observed fracture traces on given surfaces.

Numerical method

Flow is computed by a simple Galerkin finite-element scheme. A conjugate gradient method with incomplete Choleski preconditionning is used for the sparse matrix solver. Transport is computed by either particle-tracking or particule following.

Limitations

Boundary conditions do not include unconfined flow. Transport is not coupled with density effects : the density field is not modified by the transport of salt, for example. The code is best adapted to modelling transport in steady-state flow fields. Transport in transient flow fields is possible but cumbersome.

Parameters required

Geometric parameters

- shape and dimensions of the model (sphere, box shaped, or intersection of box shapes).
- statistical description of the fracture discs network : definition of fracture sets and, for each set, density, distribution of radii and orientation.

or

- for each fracture : coordinates of center, radius, orientation, and definition of the active region.
- type of channel network.
- for random channels : definition of channel sets and, for each set, density, orientation distribution on discs, length distribution.
- for regular channel grids : definition of channel sets and for each set, orientation and spacing.

Hydraulic parameters

- chanel conductances distribution. Conductances are defined as the radio of flow rate over head gradient.
- channel shape factor, defined as the ratio of length over width of the channel, or channel section
- channel storativity
- longitudinal dispersivity
- boundary conditions : imposed heads and/or fluxes, injection rates.

Type of results

. heads in nodes,

. fluxes and velocities in elements, as well as at internal (holes) or external boundaries,

. residual error in heads,

. tracer concentrations in elements and/or tracer mass flux at nodes.

Computer requirements

UNIX or VMS workstation or fast PC (486-66 or Pentium) with 32 MB RAM minimum.

User interface

The code is organized in several modules :

FMG3D : disc network generation

CHANNEL : channel network generation

TRIFLO : flow computations

TRIPAR : transport computations

DIMES : network plots

Avaibility

The codes are in-house developments, with no plans for distribution at this time.

References

for technical description:

Modélisation des écoulements et du transport dans un massif fracturé, by F. Guérin. BRGM technical note Nr 92EAU037, November 1992.

for applications:

On the Relationship between connectivity and the continuum approximation in fracture flow and transport modelling, by F. Guérin and D. Billaux. Memories of the XXIVth congress of IAH, ÅS, Oslo, 1993.

REFERENCES

BILLAUX, 1990. Hydrogéologie des milieux fracturés. Géométrie, connectivité et comportement hydraulique. Ph.D. Thesis, Ecole des Mines de Paris, BRGM document n° 186

BARTHÉLÉMY, SEBTI, SCHWARTZ, 1993. Modélisation hydrodynamique du laboratoire souterrain d'Äspö - Phase II - Simulation en régime permanent. Logiciel MARTHE. Rapport ANDRA 663 - RP BRG 93-003

FILLION and NOYER, 1994. Hydrodynamic modelling of the Äspö Hard Rock Laboratory - Rockflow code - Rapport ANDRA 663-RP BRG 94-003

GUERIN and BILLAUX, 1993. On the relationship between connectivity and the continuum approximation in fracture flow and transport modelling - XXIVth Congress "Hydrogeology of hard rocks" of International Association of Hydrogeologists.

MUNIER, 1993. Four-dimensional analysis of fracture arrays at the Äspö hard rock laboratory, SE Sweden. In Engineering Geology n° 33, pp 159-175

ROBINSON P.C., 1984. Connectivity Flow and Transport in Network Models of Fracture Media. Ph.D. thesis, Ste Catherine College, Oxford

SVENSSON, 1990. The island of Äspö. Numerical calculations of natural and forced ground water simulations. SKB - HRL PR.25-90-03

List of International Cooperation Reports

ICR 93-01
Flowmeter measurement in borehole KAS 16
P Rouhiainen
June 1993
Supported by TVO, Finland

ICR 93-02
Development of ROCK-CAD model for Äspö Hard Rock Laboratory site
Pauli Saksa, Juha Lindh,
Eero Heikkinen
Fintact KY, Helsinki, Finland
December 1993
Supported by TVO, Finland

ICR 93-03
Scoping calculations for the Matrix Diffusion Experiment
Lars Birgersson[1], Hans Widén[1],
Thomas Ågren[1], Ivars Neretnieks[2],
Luis Moreno[2]
1 Kemakta Konsult AB, Stockholm, Sweden
2 Royal Institute of Technology, Stockholm, Sweden
November 1993
Supported by SKB, Sweden

ICR 93-04
Scoping calculations for the Multiple Well Tracer Experiment - efficient design for identifying transport processes
Rune Nordqvist, Erik Gustafsson,
Peter Andersson
Geosigma AB, Uppsala, Sweden
December 1993
Supported by SKB, Sweden

ICR 94-01
Scoping calculations for the Multiple Well Tracer Experiment using a variable aperture model
Luis Moreno, Ivars Neretnieks
Department of Chemical Engineering and Technology, Royal Institute of Technology, Stockholm, Sweden
January 1994
Supported by SKB, Sweden

ICR 94-02

Äspö Hard Rock Laboratory. Test plan for ZEDEX - Zone of Excavation Disturbance EXperiment. Release 1.0

February 1994

Supported by ANDRA, NIREX, SKB

ICR 94-03

The Multiple Well Tracer Experiment - Scoping calculations

Urban Svensson
Computer-Aided Fluid Engineering

March 1994

Supported by SKB, Sweden

ICR 94-04

Design constraints and process discrimination for the Detailed Scale Tracer Experiments at Äspö - Multiple Well Tracer Experiment and Matrix Diffusion Experiment

Jan-Olof Selroos[1], Anders Winberg[2], Vladimir Cvetkovic[2]
1 Water Resources Eng., KTH
2 Conterra AB

April 1994

Supported by SKB, Sweden

ICR 94-05

Analysis of LPT2 using the Channel Network model

Björn Gylling[1], Luis Moreno[1], Ivars Neretnieks[1], Lars Birgersson[2]
1 Department of Chemical Engineering and Technology, Royal Institute of Technology, Stockholm, Sweden
2 Kemakta Konsult AB, Stockholm, Sweden

April 1994

Supported by SKB, Sweden

ICR 94-06

SKB/DOE Hard Rock Laboratory Studies Task 3. Geochemical investigations using stable and radiogenic isotopic methods

Bill Wallin[1], Zell Peterman[2]
1 Geokema AB, Lidingö, Sweden
2 U.S. Geological Survey, Denver, Colorado, USA

January 1994

Supported by SKB and U.S.DOE

ICR 94-07

Analyses of LPT2 in the Äspö HRL with continuous anisotropic heterogeneous model

Akira Kobayashi[1], Ryo Yamashita[2], Masakazu Chijimatsu[2], Hiroyuki Nishiyama[3], Yuzo Ohnishi[3]
1 Iwate University, Iwate, Japan
2 Hazama Corporation, Ibaraki, Japan
3 Kyoto University, Kyoto, Japan
September 1994
Supported by PNC, Japan

ICR 94-08

Application of three-dimensional smeared fracture model to the groundwater flow and the solute migration of LPT-2 experiment

T Igarashi, Y Tanaka, M Kawanishi
Abiko Research Laboratory, Central Research Institute of Electric Power Industry, Abiko, Japan
October 1994
Supported by CRIEPI, Japan

ICR 94-09

Discrete-fracture modelling of the Äspö LPT-2, large-scale pumping and tracer test

Masahiro Uchida[1], Thomas Doe[2], William Dershowitz[2], Andrew Thomas[2], Peter Wallmann[2], Atsushi Sawada[1]
1 Power Reactor and Nuclear Fuel Development Co., Tokai, Japan
2 Golder Associates Inc., Seattle, WA, USA
March 1994
Supported by PNC, Japan

ICR 94-10

Äspö Hard Rock Laboratory
International workshop on the use of tunnel boring machines for deep repositories
Äspö, June 13-14 1994

Göran Bäckblom (ed.)
Swedish Nuclear Fuel and Waste Management Co.
October 1994
Supported by SKB, Sweden

ICR 94-11

Data analysis and modelling of the LPT2 Pumping and Tracer Transport Test at Äspö. Tracer experiment

Aimo Hautojärvi
VTT Energy
November 1994
Supported by TVO, Finland

ICR 94-12

Modelling the LPT2 Pumping and Tracer Test at Äspö. Pumping test

Veikko Taivassalo, Lasse Koskinen,
Mikko Laitinen, Jari Löfman, Ferenc Mészáros
VTT Energy

November 1994
Supported by TVO, Finland

ICR 94-13

Proceedings of The Äspö International Geochemistry Workshop, June 2-3, 1994, Äspö Hard Rock Laboratory

Peter Wikberg (chairman), Steven Banwart (proc. ed.)

December 1994
Supported by SKB, TVO, Nirex, ANDRA, CRIEPI

ISSN 1104-3210
ISRN SKB-ICR--94/14--SE
CM Gruppen AB, Bromma 1994